



**HAL**  
open science

## Does convection-permitting simulate better rainfall distribution and extreme over Guinean coast and surroundings?

Kouakou Kouadio, Sophie Bastin, Abdourahamane Konare, Vincent Ajayi

### ► To cite this version:

Kouakou Kouadio, Sophie Bastin, Abdourahamane Konare, Vincent Ajayi. Does convection-permitting simulate better rainfall distribution and extreme over Guinean coast and surroundings?. *Climate Dynamics*, 2020, 55, pp.153-174. 10.1007/s00382-018-4308-y . insu-01821831

**HAL Id: insu-01821831**

**<https://insu.hal.science/insu-01821831v1>**

Submitted on 4 Jan 2021

**HAL** is a multi-disciplinary open access archive for the deposit and dissemination of scientific research documents, whether they are published or not. The documents may come from teaching and research institutions in France or abroad, or from public or private research centers.

L'archive ouverte pluridisciplinaire **HAL**, est destinée au dépôt et à la diffusion de documents scientifiques de niveau recherche, publiés ou non, émanant des établissements d'enseignement et de recherche français ou étrangers, des laboratoires publics ou privés.

# Climate Dynamics

## Does convection-permitting simulate better rainfall distribution and extreme over Guinean coast and surroundings?

--Manuscript Draft--

<b>Manuscript Number:</b>	CLDY-D-17-00719R2	
<b>Full Title:</b>	Does convection-permitting simulate better rainfall distribution and extreme over Guinean coast and surroundings?	
<b>Article Type:</b>	S.I. : Advances in Convection-Permitting Climate Modeling	
<b>Keywords:</b>	high resolution, WRF, West Africa monsoon, Parameterization, Rainfall, convection permitting	
<b>Corresponding Author:</b>	kouakou kouadio, Ph.D Universite Felix Houphouet-Boigny Abidjan, abidjan CÔTE D'IVOIRE	
<b>Corresponding Author Secondary Information:</b>		
<b>Corresponding Author's Institution:</b>	Universite Felix Houphouet-Boigny	
<b>Corresponding Author's Secondary Institution:</b>		
<b>First Author:</b>	kouakou kouadio, Ph.D	
<b>First Author Secondary Information:</b>		
<b>Order of Authors:</b>	kouakou kouadio, Ph.D	
	Sophie Bastin	
	Abdourahamane Konare	
	Vincent O. Ajayi	
<b>Order of Authors Secondary Information:</b>		
<b>Funding Information:</b>	German Federal Ministry of Higher Education and Research (BMBF), WASCAL	Dr. kouakou kouadio
	France Government through the Service de Cooperation et d'Action Culturelle (SCAC) (SCAC/2014/BE/002)	Dr. kouakou kouadio
<b>Abstract:</b>	<p>This research work focuses on the problem of climate simulation of rainfall over West Africa and particularly over coastal countries of the Gulf of Guinea by Regional Climate Models (RCMs). The sensitivities of Weather Research and Forecasting (WRF) Model were tested for changes in horizontal resolution (convection permitting versus parameterized) on the replication of West African monsoon for year 2014. Sensitivity test was also performed for response of rainfall to changes in microphysics (MP) and planetary boundary layer (PBL) schemes. Generally, the result shows that WRF are able to replicates rainfall distribution with an adequate representation of the dynamical features of West African monsoon system. The high-resolution (wrf-4km) shows dry bias along the coast of the Gulf of Guinea but generally outperforms wrf-24km run especially in replication of the extreme rainfall distribution. The dry bias along the coastal area is suggested to not only related to convection but mostly to microphysics and PBL parameterisation schemes.</p> <p>Differences were noticed between the dynamics of WRF and ERA-interim outputs despite the use of spectral nudging in the experiment which then suggest strong interactions between scales. These differences were observed to be restricted mainly to the low-layer monsoon flow in JJA. Both runs at 24km and 4km hardly simulate the typical diurnal distribution of rainfall. The sensitivity of WRF to MP (only sophisticated MP were tested) and PBL reveals a stronger impact of PBL than MP on rainfall distribution and the most significant added value over the Guinean coast and</p>	

	<p>surroundings area was provided by the configurations using non-local PBL scheme (as ACM2). The changes in MP and PBL schemes in general seem to have less effect on the explicit runs (wrf-4km) in the replication of the rainfall over the Gulf of Guinea and the surroundings seaboard.</p>
--	--

## Revision 2

I would like to appreciate all the contribution from the reviewer to improve this work.

### COMMENTS FOR THE AUTHOR:

Reviewer #1: Second review of the paper:

Does convection-permitting climate simulation improve the replication of rainfall distribution and extreme over Guinean coast and surroundings? by Kouadio et al.

First, I would like to thank the authors that addressed part of my previous recommendations. The paper is improved. Nevertheless, after a careful second read, I have some main comments that require substantial modifications. I recommend major revision before accepting this study. Please see below my main recommendations.

Comments about the previous review:

1- About the answers of the previous revision. The authors reply only to my question without any modification of the text. These questions are not for my personal interest but reveal a lack in the explanations and should imply clarification in the text. The authors must have to reconsider some of these previous points and clarify the main document. This is, for example, for the comments L31, L326 ...

- L31: what "representations" means here? forecasted? please clarify

**This question has been addressed in the first line of the abstract.**

**Then, the first sentence has been modified from:** "This research work focuses on the problem of representation of rainfall over West Africa and particularly over coastal countries of the Gulf of Guinea by Regional Climate Models (RCMs)." **To:**

**This research work focuses on the problem of climate simulation of rainfall over West Africa and particularly over coastal countries of the Gulf of Guinea by Regional Climate Models (RCMs).**

- Paragraph starting L247 and Figure 3: The authors discuss the results over the sea, but I am more curious concerning the explanations of the intense dipole E/W over the continent. This is maybe more important than over the Ocean because it affects directly the population.

The term Guinean Coast includes all the countries around the coast. It spread till 8N. Thus, the discussion is not only about across sea but concerns the surrounding countries. The question of dipole maybe addressed in multi-years works.

The text has been modified (L284 – 305).

“This figure 3 thus shows that indeed, the run at high resolution generally, outperforms the run at 24-km resolution over the Guinean band and southern Sahel, i.e. presents an upscaled added-value. There is however, some area where the high-resolution run seems to degrade the information instead of improving the simulation, especially over Ivorian coast, south-west of Guinea and Sierra Leone. One of the main reason would be related to the fact that the better skills of the explicit run are expected at daily and sub-daily scales and for extreme values while this AV is computed over 9 months. At seasonal scale, variability is mainly driven by large-scale dynamics that is not necessary improved by the higher resolution. On the other hand, Figure 2 has shown that in comparison to TRMM and CHIRPS datasets, WRF has good performance across near-Sahel and Sahel (north of 8°N), but strongly underestimates precipitation across the coastal area of the surrounding countries of the Gulf of Guinea and mainly over the sea during the pre-onset period and at the end of the rainy season. This leads to strong dry bias from the sea to about 6N (beyond the coast) during the rainy season over Sahel. One may suggest that the introduction of this dry bias along the Gulf of Guinea seaboard toward the equator (from 5°N and equatorward) into the model simulations (either parameterized and explicit convection), may be directly related to the forcing conditions. Moreover, previous works as Meynadier et al. (2010) and Marsham et al. (2013) revealed that the southward bias in the simulation of rainfall across West Africa, is an inherent problem for RCMs. Thus, model parameterisation schemes can be point out. Furthermore, convection-permitting simulation seems not to be able to correct effectively the dry bias. Therefore, convective parameterization alone may not be enough to

explain this dry bias. Klein et al. (2015) found a similar dry bias in a cumulus, microphysics and boundary layer parameterization ensemble analysis of WRF version 3.5.1 and related it to the driving conditions.”

- L268: gridded data means observed here? please clarify

The paragraph has been removed.

However, it was related to: “reliable and long-term daily observed gridded data”

- Paragraph starting L268 and Figure 4: The direct comparison between station datasets....

The section has been removed. The suggested plot can be seen in figure 5.

- Paragraph starting L316 useless and questionable, I recommend to remove it

The section has been removed as suggested

- L324: Please clarify the reason of this specific box

This clarification can be found in the text: L213-L318;

“This box is based (1) on the availability of ground-based observation which did not spread over the whole region and also (2) to allow for better comparison of previous works as Klein et al. (2015) and those that focused on onset like Sultan and Janicot (2000, 2003).”

- L326: 25th percentile of the rainy days (conditional) or of all the days?

The answer can be found in the text at line: L322-L324;

“It is worth noting that all the non-rain events have been beforehand removed in order to consider only the statistics based on effective rain events.”

- L328: Could the authors explain how the regrid of the data can generate positive then negative changes of precipitation depending the hours of the day. It is not clear to me.

The section has been modified: L313-364

- Paragraph starting L332 is too descriptive.

The paragraph has been adapted: L313-364

- Subsection 3.4 is also too descriptive. Please synthesize.

The section has been modified and figure changed: Subsection 3.3

- L383: The authors write "it provides more realistic estimations over the Sahel and emphasizes the benefit of the high-resolution simulation." But this is too speculative. The justifications are too few and based only on one figure that is not well adapted, and on one specific quantile.

The graph has been adapted to support the statement section 3.3

- L394: This is too specula

The graph has been adapted to support the statement. section 3.3

- Paragraph starting L397: I recommend to remove this paragraph.

removed previously

- L454 Ivory Coast

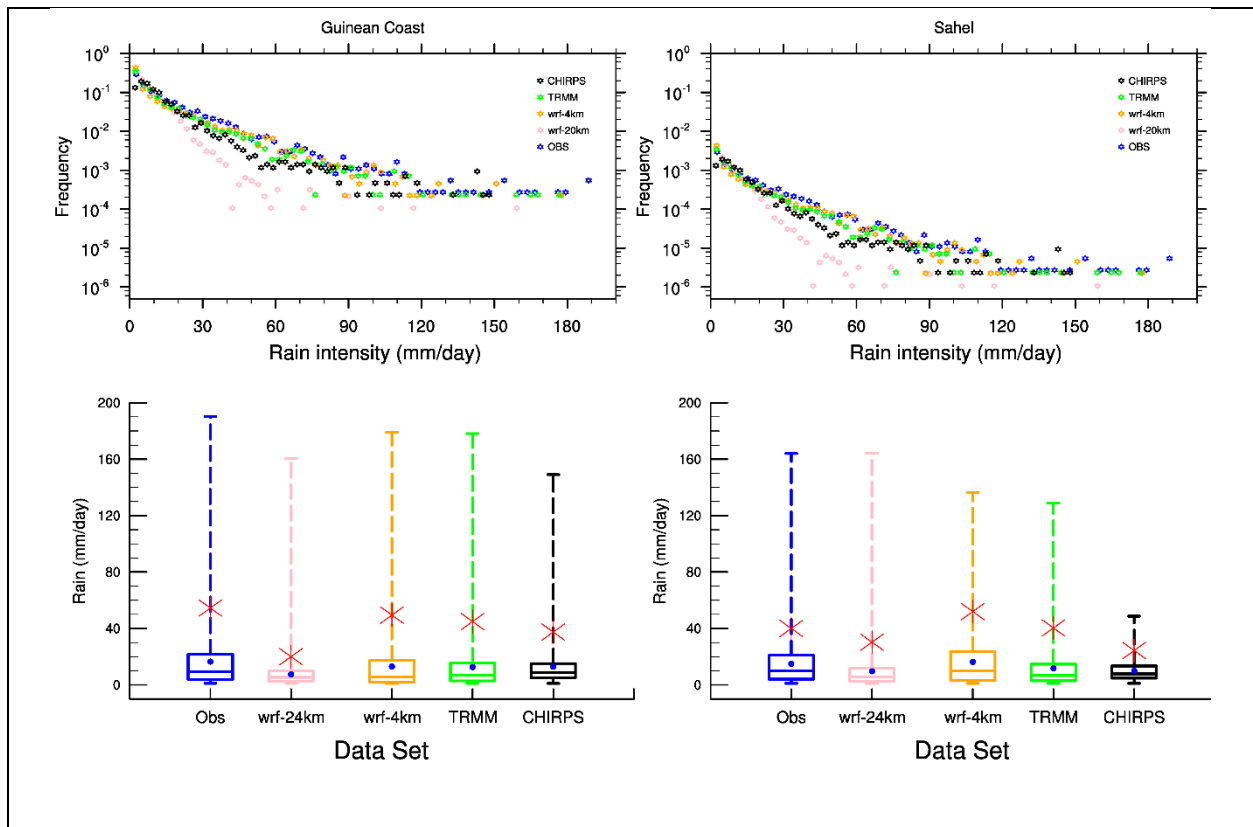
Corrected: L500, L279, L280

2- About the scientific results and the impacts of the resolution. I am still convinced that most of the difference in term of precipitation values between WRF-24km and WRF-4km are explained by the size of each cells associated with each grid point (i.e. downscaling effect and not necessary a physical impact of the schemes). The authors should reconsider their methodologies to better prove these impacts. For example, what are the results of the new Fig. 5 if the authors would use the same resolution (by upscaling the WRF-4km simulation). Will they find results significantly different?

Figure 5 has been repeated with the regridded wrf-24km and wrf-4km into TRMM dataset grid scale. It is noticed from the analysis marginal differences between WRF native and regridded rainfall output at daily scale. The discussion can be found in the text at: L423-L432. The figure is added just after

Similar analysis has been made at diurnal scale (L313:L364), and the result indicate that: upscaling WRF outputs into the grid scale of TRMM dataset has an effect on the number of the events regardless of the range of rainfall intensity, however, the timing is preserved.

Thus, results may suggest a combination of both grid scale factors and physics on the observed differences between the runs at 24km (parameterized convection) and 4km (convection-permitting).



Empirical probability distribution functions of daily precipitation (top) daily. Boxplots of the daily precipitation (Bottom) respectively from the ground-based observations, wrf-24km, wrf-4km, TRMM and CHIRPS data sets over the Guinean coast (left) and the Sahelian (right) regions. The boxes indicate respectively from the bottom to the top the first, second and third interquartile ranges and the whiskers stretch to minimum and maximum values of each data set. Blue dots and the red stars represent respectively the mean value and the 95<sup>th</sup> percentile of the precipitation for each data set. Wrf-24km, wrf-4km and CHIRPS datasets have been upscale into TRMM grid scale.

This comment seems more important in this second round since the difference between the two simulations in the new Fig. 6 and 7 are not very different. By the way, are these differences significant?

3- Despite some main comments of the previous review, some figures (see details below) have a too low quality relative to the standard of this journal. The authors have to improve most of them, and should be careful with the titles, axis, captions.

Main comments on the new document:

Abstract: To me the justification of this study, and more specifically why only PBL and MP schemes are the only schemes analysed, is not well exposed. Also, the authors are still using some speculative, or at least not justified, conclusions such as 'fairly replicates', 'good simulation'. These conclusions should be better assessed with significant test. As a reminder, this study uses only one year that reduces considerably the significance of the results, the authors should be as cautious as possible.

The limitation of the study related to the specific year has been mentioned at the end of the conclusion and the abstract has been revised.

Section 3.1:

Still too long and descriptive. For example, paragraph starting L284 must be simplified.

L 293: 'Moreover, ERAI allocated shows its maximum precipitation toward the south' sounds weird to me

Paragraph L226-L239 of the previous version has been removed and the section has been modified to consider among other remarks the upscale of wrf-4km aspect.

Paragraph starting L284 has been modified. L270-L297

Section 3.2:

There are some confusions when the authors discussed the quantiles of precipitation (Q95). Sometimes they are using the value of Q95 in the observation, sometimes they are using this thresholds for each dataset. Please avoid mixing up the two methods.

The section has been modified and it also consider the upscale of wrf-4km.

Only L338-L340 mentioned Q95 using wrf-24km to discuss about the marginal occurrence of intense rain events with wrf-24km.

L349. No ERAI is not used any more in this figure, please correct.

This has been corrected: L355

L363: The underestimation of the model (especially with the 24-km resolution) is quite logic. That should be mentioned.

Paragraph starting L363 and Figure 5. To me, the effect of the downscaling effect of the precipitation is the main driver of the results. The authors should compare the precipitation at the same resolution.

All the datasets have been upscaled to TRMM grid scale. The plot shows negligible changes and the result has been discussed on the text: L409:418. See figure added in this report.

Section 4.1 and figure 6 and 7. Could the authors check carefully what they plot and discuss. In the title, caption and in the text, they mention the difference, but to me it is not. Please reconsider all this part.

The section has been modified L426-477. Differences can be observed between ERAI and WRF outputs especially at lower levels. For example, in the northern extend and intensity of monsoon flow, the intensity of African easterly Jet and the location and intensity of deep convection.

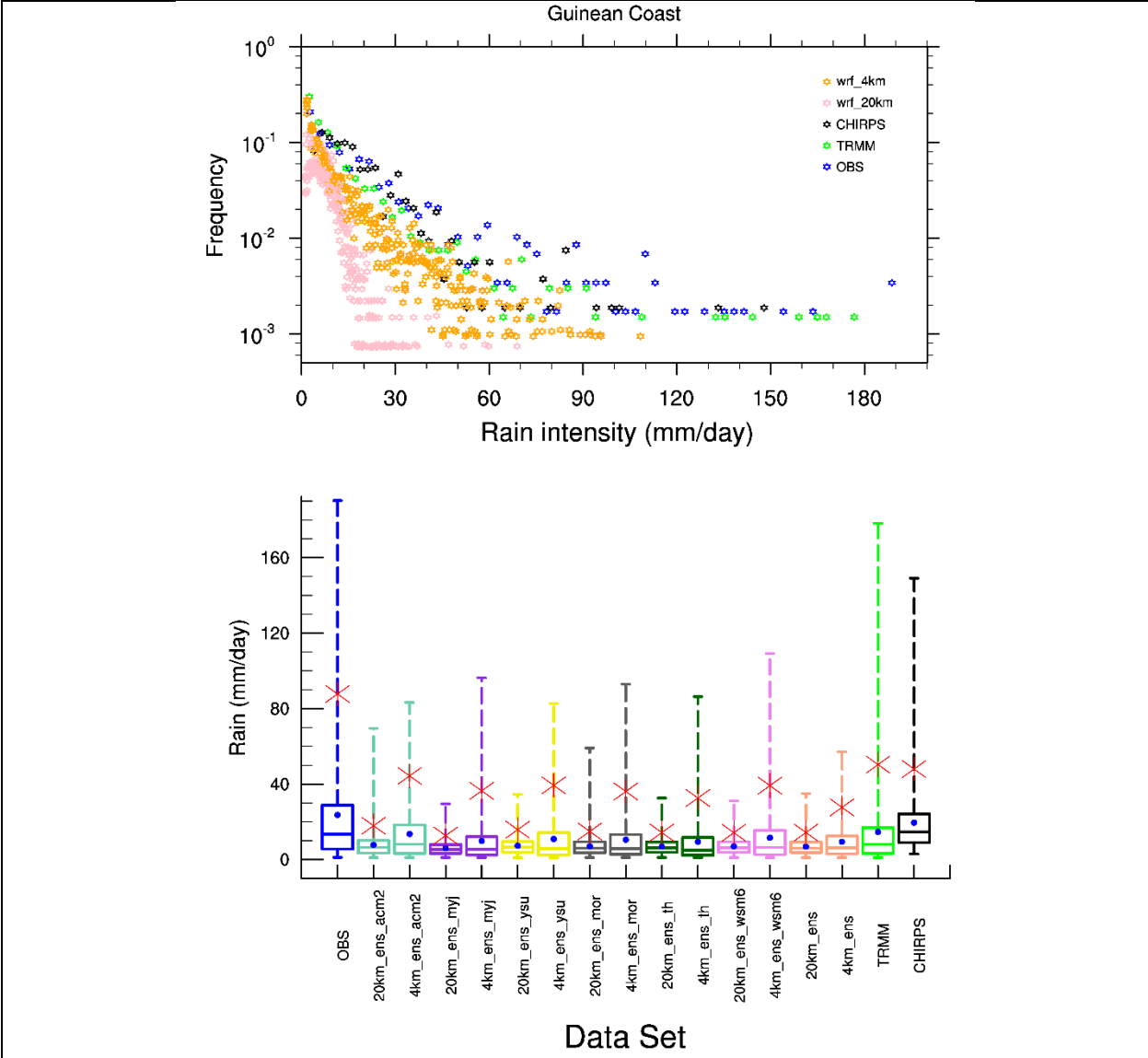
Less important differences are observed between wrf-24km and wrf-4km and wrf-4km seems closer to ERAI.

At the end of the section 4.1, what are the conclusion of these difference. Do they authors consider the WRF-4 is better than WRF-24. This section is still too descriptive, general comments and main conclusions are missing.

The differences between wrf-24km and wrf-4km are not pronounced enough to fully consider that wrf-4km is better wrf-24km however, the explicit run shows result closer to the ERAI.

Paragraph starting 517: To me the results are mainly explained by the resolution of each product. Please use the same resolution to fairly compared these datasets.

Figure 8 has been rebuilt using the regridded wrf-24km and wrf-4km into TRMM dataset grid scale. As figure 5 there is marginal changes and we have same conclusion.



Empirical probability distribution functions of daily precipitation (top) daily. Boxplots of the daily precipitation (Bottom) over the Guinean coast (left) and the Sahelian (right) regions. Boxplots of the daily precipitation over the Guinean coast respectively from the ground-based observation, TRMM, ERA-interim and wrf-24km, wrf-4km from each ensemble group members of the different configurations. The boxes indicate respectively from the bottom to the top the first, second and third interquartile ranges and the whiskers stretch to minimum and maximum values of each data set. Blue dots and the red stars represent respectively the mean value and the 95 percentiles of the precipitation for each data set. Wrf-24km, wrf-4km and CHIRPS datasets have been upscale into TRMM grid scale.

Figures:

Fig 4: The quality of these figures could be improved. No need of title for each panel (this should be indicated in the caption). Legend not readable and only one is required.

The figure has been modified

Figure 5, where are the numbers mentioned at the end of the caption

Corrected

Figure 6 and 7 Difference, are you sure?

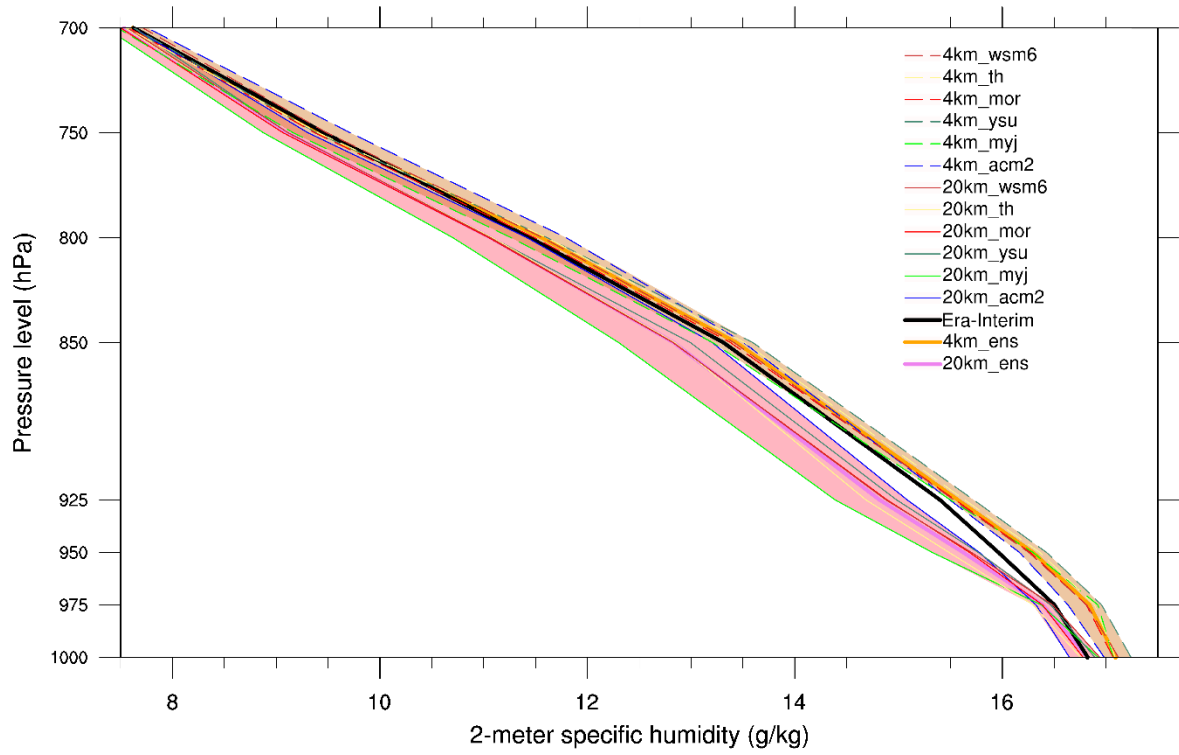
Already answer in previous comments

Figure 7 Please keep the same structure as in Fig 6 (first column ERAI, second WRF-4, third WRF-24)

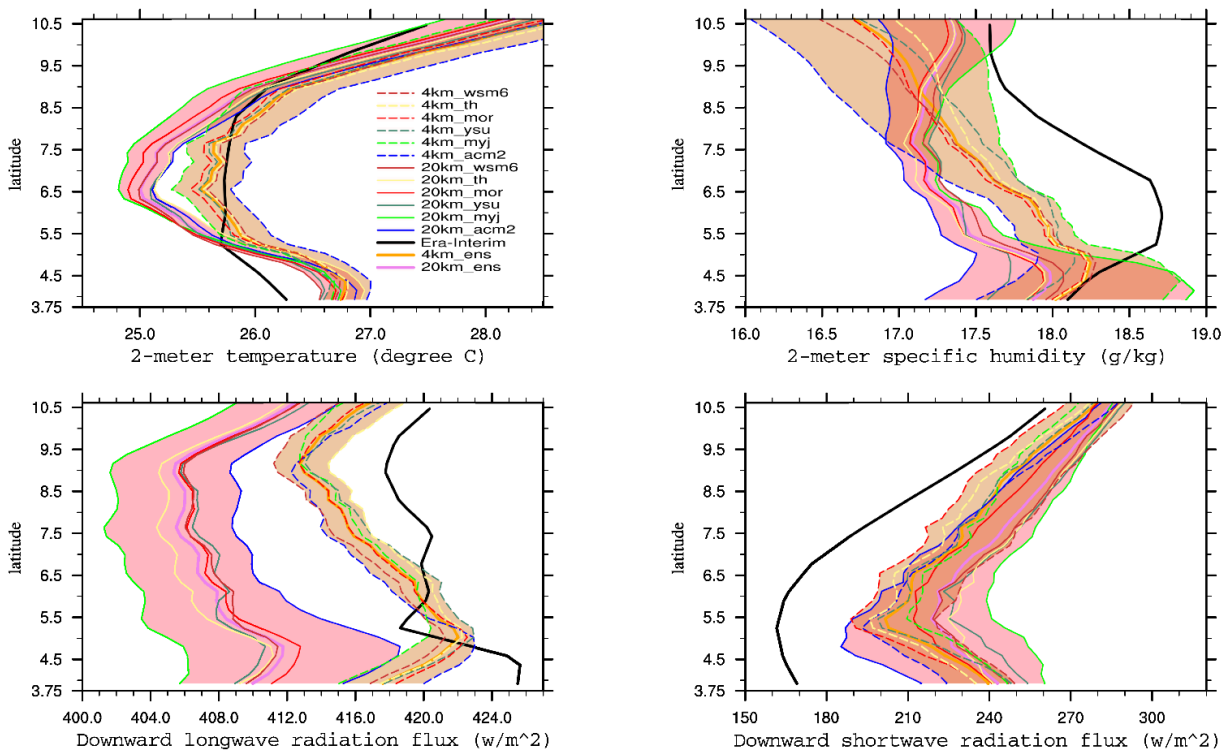
The figures 6 and 7 have modified accordingly (first column ERAI, second WRF-4, third WRF-24)

Figure 9 and 10 not readable, low quality, need to be synthesized

The Figures 9 and 10 give detail information about the ensembles. It therefore going to be difficult to regroup them without missing the information. The quality of the graphs has been improved.



**Fig. 9** Vertical profiles of specific humidity from wrf-20km and 4km sub-ensembles group members and Era-interim data set. All the values are averaged from 10W to 5E. The pink and orange coloured areas mark the range of value respectively with wrf-24km and wrf4km.



**Fig. 10** Meridional evolution of 2-meter temperature, specific humidity, downward shortwave and longwave radiation fluxes from wrf-20km and 4km ensemble group members and from Era-interim data set. All the values are averaged from 10W to 5 E. The pink and orange coloured areas mark the range of value respectively with wrf-24km and wrf4km.

Figure 12 is mentioned very briefly, consider to remove it.

The figure has been removed



33 **Abstract**

34 This research work focuses on the problem of climate simulation of rainfall over West Africa and  
35 particularly over coastal countries of the Gulf of Guinea by Regional Climate Models (RCMs).

36 The sensitivities of Weather Research and Forecasting (WRF) Model were tested for changes in  
37 horizontal resolution (convection permitting versus parameterized) on the replication of West  
38 African monsoon for year 2014. Sensitivity test was also performed for response of rainfall to  
39 changes in microphysics (MP) and planetary boundary layer (PBL) schemes. Generally, the result  
40 shows that WRF are able to replicates rainfall distribution with an adequate representation of the  
41 dynamical features of West African monsoon system. The high-resolution (wrf-4km) shows dry  
42 bias along the coast of the Gulf of Guinea but generally outperforms wrf-24km run especially in  
43 replication of the extreme rainfall distribution. The dry bias along the coastal area is suggested to  
44 not only related to convection but mostly to microphysics and PBL parameterisation schemes.

45 Differences were noticed between the dynamics of WRF and ERA-interim outputs despite the use  
46 of spectral nudging in the experiment which then suggest strong interactions between scales. These  
47 differences were observed to be restricted mainly to the low-layer monsoon flow in JJA. Both runs  
48 at 24km and 4km hardly simulate the typical diurnal distribution of rainfall. The sensitivity of  
49 WRF to MP (only sophisticated MP were tested) and PBL reveals a stronger impact of PBL than  
50 MP on rainfall distribution and the most significant added value over the Guinean coast and  
51 surroundings area was provided by the configurations using non-local PBL scheme (as ACM2).  
52 The changes in MP and PBL schemes in general seem to have less effect on the explicit runs (wrf-  
53 4km) in the replication of the rainfall over the Gulf of Guinea and the surroundings seaboard.

54

55 **Key words:** high resolution, WRF, West Africa monsoon, Parameterization, Rainfall, convection  
56 permitting

## 57        **1. Introduction**

58            The West African region which extends from the Gulf of Guinea to the Sahel is an area  
59 which is subjected to alternating dry and wet seasons mainly linked to the monsoon, which  
60 influences the majority of annual precipitation. This region is an important source of aerosols and  
61 energy, which contributes to the formation of tropical cyclones. Therefore, this region greatly  
62 interacts with the Earth climate system and has been subject of numerous studies (Fontaine and  
63 Philippon 2000; Trenberth *et al.* 2000 ; Ali *et al.* 2005 ; Abiodun *et al.* 2008 ; Konare *et al.* 2008  
64 ; Druyan *et al.* 2010 Moufouma-Okia and Rowell 2010 ; Sylla *et al.* 2010b ; Flaounas *et al.* 2012).  
65 West African region has also been identified as one of the poorest region in the world which  
66 depends mainly on rain-fed agriculture and one of the most vulnerable to climate change and  
67 climate variability (IPCC 2007). This vulnerability is aggravated by the interaction of ‘multiple  
68 stresses’ (drought frequency and duration, frequency of extreme events, among others), occurring  
69 at various levels, and the low adaptive capacity (IPCC 2007). Several studies (Omosho *et al.*  
70 2000; Sultan and Janicot 2000, 2003; Hagos and Cook 2007; Omosho 2008; Pm. Ruti 2009;  
71 Janicot *et al.* 2010; Oettli *et al.* 2011) have argued that seasonal forecast of rainfall is crucial for  
72 socio-economic development in this sub-region. This is in the aim to (i) prevent extreme events  
73 like floods in the southern part, (ii) management of climate risk in agriculture (better preparedness  
74 for rain-fed agricultural activities), (iii) forestall outbreak of diseases in the Sahel region etc.

75            Although many studies have focused on the prediction of the rainfall, there exists  
76 challenges of reliable seasonal forecast due to several forcings. For example, the climate of this  
77 region is influenced by the interactions of various complex mechanisms (topography, ocean-  
78 atmosphere interactions, atmosphere-biosphere exchanges etc.). In order to address these issues,  
79 several studies investigated the patterns of inherent variability in the West African monsoon at  
80 intra-seasonal, seasonal and interannual scales with the purpose to better understand the West  
81 African Monsoon (WAM) mechanisms (Adedoyin 1989; Nicholson 2001; Brooks 2004; Okumura  
82 and Xie 2004; 2004, Steiner *et al.* 2009 ; De Coëtlogon *et al.* 2010 ; Fink *et al.* 2010 ; Gbobaniyi  
83 *et al.* 2014 ; Meynadier *et al.* 2014) and precipitation characteristics (location, intensity, duration  
84 *etc.*).

85            The relationship between rainfall and regional or large-scale dynamics over West Africa  
86 has been reported by earlier studies (Nicholson and Grist 2003; Sultan *et al.* 2003). The onset of

87 the monsoon is associated with the intensification of the Tropical Easterly Jet (TEJ), a northward  
88 shift and a weakening of the African Easterly Jet (AEJ), which is associated with a decrease of  
89 African Easterly Waves (AEWs) activity (Lavaysse et al. 2006; Sylla et al. 2010b). These results  
90 are in agreement with observation of Omotosho (2008) which found a stronger AEJ during dry  
91 years than during wet ones. Air-sea (through the Sea Surface Temperature (SST) in the Gulf of  
92 Guinea) interactions also play an active role in the amount of precipitation, its spatial distribution  
93 and northward migration (Leduc-Leballeur et al. 2013). (Vizy 2002) investigated the influence of  
94 the Gulf of Guinea's SST anomalies (SSTAs) on the climatology of the WAM and found an  
95 increase in rainfall over the Guinean coast area as a result of an increment in the lower tropospheric  
96 water vapour content due to increased evaporation over the warm SSTAs. This was accompanied  
97 by a decrease in rainfall over the southern Sahel. More generally, (Gaetani et al. 2017) have shown  
98 that the SST warming affects the Sahelian precipitation through modifications in the global tropical  
99 atmospheric dynamics, reducing the importance of the regional drivers. (Flaounas et al. 2012) and  
100 (Mohino et al. 2011) also linked the onset and the different phases of precipitation over West  
101 Africa to the convection over India and Indian ocean that generates Rossby waves which favors  
102 the occurrence of dry air intrusion over West Africa, inhibiting convective activity. And finally,  
103 the heat low dynamics has been shown to strongly influence the onset of the monsoon and its intra-  
104 seasonal variability (Lavaysse et al. 2009, 2010a, b), but also its variability at longer time scales  
105 due to radiative effects of water vapor that affect the regional dynamics (Evan et al. 2015). The  
106 increase of CO<sub>2</sub> in the atmosphere also affects the precipitation at regional scale (Gaetani et al.  
107 2017). An overview of the monsoon and its relationship with the climate system of the region is  
108 provided by Nicholson (2013).

109 All these efforts in addition to constant progress of models are expected to allow adequate  
110 representation of the WAM. However, at present day, models still have many difficulties to  
111 simulate the West African climate features. Several reasons are suggested to justify these  
112 underperformances ranging from the physics of the models, scale interactions, lacks of reliable  
113 and dense observation data suited to the resolution of the models. For example, Chang (2011)  
114 proposed that the limitation of climate models to reproduce the diurnal, seasonal and annual cycles  
115 of the rainfall over West Africa is related to a limited capacity of meteorological services in getting  
116 observations data set, and human and informatics resources. Indeed, the complex coupled systems  
117 that modulate climate system of the region are not well incorporated in current models, and one

118 reason is that in most studies, precipitation is considered at monthly and regional scales, while  
119 precipitation over this area have a very strong variability when looking at higher temporal and  
120 spatial scales, with most of events occurring in the tails of classical precipitation distribution (either  
121 very intense events, either dry periods). Furthermore, Intergovernmental Panel on Climate Change  
122 (IPCC) acknowledged on its Third Assessment Report (TAR) that a model run at coarse resolution  
123 does not allow detailed extreme rainfall evaluation (Griggs and Noguer 2002). Then the simulation  
124 of the WAM at very high resolution is suggested to have a positive impact on the representation  
125 of the West African Climate, not only because the physical processes will likely be better  
126 represented but also because the explicit convection may help in the reproduction of this kind of  
127 distribution (Ban et al. 2014; Prein et al. 2015). However, some model improvements are likely  
128 necessary but the lack of observations to well define the distribution does not make the task easy.

129         Some earlier studies (Gallée et al. 2004; Doi et al. 2012; Holloway et al. 2012; Patricola et  
130 al. 2012; Marsham et al. 2013; Moufouma-Okia and Jones 2014; Small et al. 2014; Harlaß et al.  
131 2017) showed an improvement of their simulations using high resolution simulation. Marsham *et*  
132 *al.* (2013) investigated the role of the moist convection over West Africa throughout a comparative  
133 study based on a horizontal resolution's cascade simulations using the UK Met Office Unified  
134 Model (UM). The runs are composed of grid spacing's of 4 and 12 km for 25 July to 4 August  
135 2006. The first run is done with a convective parameterization and the second with an explicit  
136 convection. They found a better representation of the WAM with the explicit run. The major  
137 improvements come from a more realistic estimation of the latent and radiative heating in the  
138 northern part of West Africa and a better representation of the diurnal cycle of the rainfall. They  
139 noticed that these representations weaken the monsoon flow, the Sahel-Sahara pressure gradient,  
140 delaying the related diurnal cycle and modifying the interaction between monsoon and the  
141 boundary layer convection. They further reported that this result raises the importance of the  
142 interaction between monsoon and convection. In addition to the explicitly resolving of deep  
143 convection, convection-permitting run also allow a better representation of fine-scale orography  
144 and variations of surface fields. This is really important in mountainous regions and in areas with  
145 heterogeneous land surfaces like coastal and urban regions, wetlands, and patchy land covers.  
146 Therewith, resolving fine-scale surface heterogeneity is also of paramount importance due to the  
147 fact that it is an important forcing for deep convection (Prein et al. 2015).

148           However, the high-resolution simulation of the WAM remains largely under explored  
149 because such type of high resolution modelling works requires high computational resources,  
150 innumerable computing time, and processors to high storage capacity. As a consequence, the  
151 studies conducted on the analysis of the WAM at high resolution are still too short (e.g. 11 days  
152 for Marsham *et al.* (2013)) to fully make a conclusion for a model in a climate mode, when the  
153 impact of the initial state will be cancelled. Therefore, the analysis of the WAM at very high  
154 resolution remains an important concern. In addition, the prevention of events with high social,  
155 economic and environmental impacts remains a constant challenge over the region. There is a  
156 need for identification of accurate models with optimal parameterizations for better understanding  
157 of the processes which allow a better prediction of West African rainfall variability and extreme  
158 and then provide the best way of using of regional dynamical model as a forecast tool and  
159 overcoming the difficulties of explaining the detailed rainfall and intense rainfall process over the  
160 West African region and particularly along the Guinean Coast and surrounding.

161           The study presented here evaluates the added-value of performing a convective permitting  
162 simulation in a climate mode, covering a longer period than a case study (several months) for the  
163 representation of rainfall distribution over Guinean coast, with a focus on heavy rainfall. Several  
164 combinations of parameterization schemes are compared in this explicit convective climate mode  
165 and the best combinations for replication of high rainfall events over Guinean Coast and  
166 surroundings are proposed. Section 2 describes the model and experiments which are compared  
167 and evaluated in section 3. Section 4 assesses the role of dynamics and physics in the performance  
168 of the different simulations. Finally, section 5 concludes the study.

169

## 170           **2. Model Description and Experiments**

171           Weather Research and Forecasting (WRF) Model is used in this study to first assess the  
172 capability of High-Resolution Regional simulation (convective-permitting) of West African  
173 Climate.

174           The first set of simulations uses two nested domains over the West African region (Fig.1)  
175 from March to September 2014. The coarser domain extends from 25°W to 30°E and from 10°S  
176 to 40°N with 24km horizontal resolution. The inner domain is one-way nested from 17°W to 10°E

177 and from 4°N to 20°N run at 4km horizontal resolution (figure 1, black rectangle). Lateral  
178 boundaries of the 24km domain are forced with Centre for Medium-Range Weather Forecasts  
179 (ECMWF) reanalyses ERA-interim (Dee et al. 2011) and it is spectrally nudged towards ERA-  
180 interim for wavelength of 1680 km in the zonal direction and of 1576 km in the meridional one to  
181 avoid unrealistic departures from the driving fields due to the size of the domain (Stauffer and  
182 Seaman 1990; Salameh et al. 2010; Omrani et al. 2012). The nudging concerns zonal and  
183 meridional wind and the temperature above the boundary layer. The configuration of WRF model  
184 includes 51 vertical layers extending up to 50 hPa, and uses the Yonsei University (YSU) planetary  
185 boundary layer scheme (Hong et al. 2006), the Noah land-surface model (Chen and Dudhia 2001),  
186 the Rapid Radiative Transfer Model for Global models (RRTMG) for shortwave (Dudhia 1989)  
187 and longwave (Mlawer et al. 1997) and the single-moment six-class (WSM6) grid-scale  
188 microphysics scheme (Hong and Lim 2006). Both domains share the same physics  
189 parameterizations except that in the nested domain, cumulus (CU) parameterization is not activated  
190 to allow explicit convection. The Kain–Fritsch (KF) convective scheme is used in the coarse  
191 domain with activation of interaction with RRTMG to take into account subgrid-scale radiative  
192 effects of clouds according to Alapaty *et al.* (2012), Herwehe *et al.* (2014).

193         The second set of runs is performed to focus on the physical processes of rainfall over the  
194 Guinean Coast, particularly on the influence of microphysics and boundary layer processes on the  
195 simulation of intense precipitations. These experiments consist of an ensemble of runs combining  
196 different boundary layer and microphysics schemes. Nudging is used in the coarse domain to  
197 ensure that the large-scale dynamics is the same in all the simulations of the ensemble. Table 1  
198 provides a summary of the schemes used and the different experiments. For this second set of  
199 simulations, only one month is run (June 2014), over the domains shown by pink boxes in Fig.1.  
200 Resolutions of the two nested domains are 20 km and 4km respectively. The nested domain focuses  
201 on the southern coastal area of West Africa.

202         An inter-comparison of the model outputs from these different configurations versus  
203 observation data is performed to find the best configuration that may provide an optimal  
204 representation of rainfall/heavy rain over West Africa in general and particularly over the Guinean  
205 Coast area. Observations come from satellites, ground-based stations and reanalyses. The ground-  
206 based data used here are daily records of temperature and precipitation over 74 stations across  
207 West Africa where the data are available for the year 2014 and selected according to the

208 geographical position. The precipitation product from Tropical Rainfall Measuring Mission  
209 (TRMM) version 3B42V7 (3-hourly, daily) allows to cover the entire area with a 0.25° spatial  
210 resolution (Huffman *et al.* 2007). In addition to TRMM data set, the Climate Hazards Group  
211 InfraRed Precipitation with Station data (CHIRPS) rainfall dataset is used. This dataset is spanning  
212 50°S-50°N (and all longitudes), starting in 1981 to near-present, CHIRPS incorporates 0.05°  
213 resolution satellite imagery with in-situ station data to create gridded rainfall (Funk *et al.* 2015).

214 Specific humidity and temperature at 2-m, shortwave and longwave downward radiation  
215 fluxes are also compared with ERA-Interim (at 0.75°x0.75° spatial resolution). Because of the  
216 limitation of the precipitation derived from ERAI as discussed by Di Giuseppe *et al.* (2013), the  
217 results with this dataset is not shown in the following graphs.

### 218 **3. Evaluation of the estimated rainfall**

#### 219 **3.1 Seasonal analysis**

220

221 The simulation of rainfall by Regional Climate Model (RCM) over West Africa is still a  
222 full challenge as reported in many previous studies such as Marsham *et al.* (2013) ; Meynadier *et*  
223 *al.* (2014) ; Birch *et al.* (2014) and Panitz *et al.* (2014). Laprise *et al.* (2008) and Di Luca *et al.*  
224 (2012) stated that the initial concept of the nesting technique is to use RCMs like sophisticated  
225 “magnifying glasses” where “the generated small scales accurately represent those that would be  
226 present in the driven data if they were not limited by resolution”. In this section of the work, the  
227 general improvement in the simulation of rainfall over West African region is assessed. Hereafter  
228 the terms wrf-24km and wrf-4km are used to identify respectively results from runs at 24km and  
229 4km respectively.

230 The seasonal evolution of the rain belt is displayed on Figure 2 as a time-latitude diagram  
231 of 5-days run mean of precipitation averaged between 10°W-10°E. The date of the onset is  
232 determined here by the transitional phase when precipitation decrease over the southern area  
233 around 5°N followed by its intensification northwards as indicated by Sultan and Janicot (2000,  
234 2003) and followed by Flaounas *et al.* (2012). It can be more or less pronounced, depending on  
235 the year.

236 The proposed oceanic phase by De Coëtlogon et al. (2010) and Leduc-Leballeur et al. (2011, 2013)  
 237 is shown in both TRMM and CHIRPS dataset. From April to end of May, maxima of precipitation  
 238 are generally located to the south 5°N and moved to around 5°N belt till it jumps northwards in  
 239 mid-July. This first phase of the monsoon latitudinal and seasonal displacement is not well  
 240 reproduced by both as WRF outputs estimate the maxima of rainfall over land even during spring.  
 241 This premature inland incursion of rainfall belt generates wet bias over land and dry bias over the  
 242 ocean and coastal region during spring and June. After the pre-onset period, both CHIRPS and  
 243 TRMM show a weakening of the rainfall in early July and it is followed by a fair recovery with a  
 244 maxima core around 7°N before moving northward. Thus, July 9<sup>th</sup> can reasonably be chosen as  
 245 Sahelian onset date with TRMM and CHIRPS. In WRF, the monsoon rainfall belt moves  
 246 northwards but lower than CHIRPS and TRMM data. It is then difficult to define a day for the  
 247 onset with the model simulations. The farthest inland penetration is observed August 15<sup>th</sup> and this  
 248 is replicated by both the observational datasets and WRF simulation. It is pertinent to note that the  
 249 observations (especially CHIRPS) show that during this period of maximum precipitation over  
 250 Sahel, there is a significant precipitation events along the Guinean Coast while WRF simulation  
 251 replicates a dry condition. After this date, the rainfall belts retreat gradually equatorward.

252 To assess the spatial value addition of the high resolution run as against the ‘coarse  
 253 resolution run’ and both WRF simulations as against ERA-interim (not shown), we computed the  
 254 added value (AV) based on the equation (1) proposed by Di Luca *et al.* (2013) and modified by  
 255 Dosio *et al.* (2014):

$$256 \quad AV = \frac{(X_{mod1} - X_{OBS})^2 - (X_{mod2} - X_{OBS})^2}{\text{Max}((X_{mod1} - X_{OBS})^2, (X_{mod2} - X_{OBS})^2)} \quad (1)$$

257

258 where X is the tested variable (here precipitation), the index mod1 is for the model with the coarser  
259 resolution, the index mod2 for the simulation at higher resolution and OBS for Observations from  
260 TRMM and CHIRPS. The AV is computed over the 9 months and all data are regridded over the  
261 same grid (TRMM). Then the average value of AV for each grid point over the total period is  
262 plotted on Figure 3. AV is positive where model#2's squared error is smaller than the model#1's  
263 one and negative otherwise. The positive values (cool colours) suggest an improvement of  
264 representation by the model#2 and the negative (warm colours) indicate where model#2 degrades  
265 the information provided by the model#1. In this figure, the added value of wrf-4km to wrf-24km  
266 is computed using both TRMM (top) and CHIRPS (bottom) as reference dataset. The value  
267 addition of the wrf-4km as against wrf-24km which allows the evaluation of the usefulness of  
268 convective-permitting run, indicates an improvement of the simulation of average rainfall using  
269 the explicit run in comparison to wrf-24km in the half north of **Ivory Coast**, Ghana, Benin and part  
270 of Nigeria. On the contrary, the area westwards of **Ivory Coast** towards southwards of Senegal  
271 indicate that WRF-24km performs better. Above 14°N, the signal is too weak to allow a  
272 conclusion. There is a very good agreement between the value added computed based on either on  
273 TRMM or CHIRPS dataset.

274 This figure 3 thus shows that indeed, the run at high resolution generally, outperforms the  
275 run at 24-km resolution over the Guinean band and southern Sahel, i.e. presents an upscaled added-  
276 value. There is however, some area where the high-resolution run seems to degrade the information  
277 instead of improving the simulation, especially over Ivorian coast, south-west of Guinea and Sierra  
278 Leone. One of the main reason would be related to the fact that the better skills of the explicit run  
279 are expected at daily and sub-daily scales and for extreme values while this AV is computed over  
280 9 months. At seasonal scale, variability is mainly driven by large-scale dynamics that is not  
281 necessary improved by the higher resolution. On the other hand, Figure 2 has shown that in  
282 comparison to TRMM and CHIRPS datasets, WRF has shown result closed to the observation  
283 across near-Sahel and Sahel (north of 8°N), but strongly underestimates precipitation across the  
284 coastal area of the surrounding countries of the Gulf of Guinea and mainly over the sea during the  
285 pre-onset period and at the end of the rainy season. This leads to strong dry bias from the sea to  
286 about 6N (beyond the coast) during the rainy season over Sahel. One may suggest that the  
287 introduction of this dry bias along the Gulf of Guinea seaboard toward the equator (from 5°N and  
288 equatorward) into the model simulations (either parameterized and explicit convection), may be

289 directly related to the forcing conditions. Moreover, previous works as Meynadier et al. (2010 and  
290 Marsham et al. (2013) revealed that the southward bias in the simulation of rainfall across West  
291 Africa, is an inherent problem for RCMs. Thus, model parameterisation schemes can be point out.  
292 Furthermore, convection-permitting simulation seems not to be able to correct effectively the dry  
293 bias. Therefore, convective parameterization alone may not be enough to explain this dry bias.  
294 Klein et al. (2015) found a similar dry bias in a cumulus, microphysics and boundary layer  
295 parameterization ensemble analysis of WRF version 3.5.1 and related it to the driving conditions.  
296 Here, if this dry bias could be related to a narrow north-south extent of the rain belt in WRF  
297 specially in WRF-24km as discussed in Klein *et al.* (2015) it may be mostly related to the  
298 microphysics and boundary layer parameterizations and not only to cumulus parameterization as  
299 already suggested in Flaounas, et al. (2011) and Klein et al. (2015). This result motivated the  
300 second set of runs, but this will be discussed later because we will first evaluate the impact of  
301 convective-permitting simulations at higher time scales.

### 302 **3.2 Rainfall diurnal cycle**

303 Figure 4 shows the diurnal cycle of rainfall occurrences over the Gulf of Guinea sub region  
304 for different categories of events based on their intensity. The 3-hourly average rainfall of each  
305 dataset is computed over the considered region (4N-8N; 10W-10E). This box is based (1) on the  
306 availability of ground-based observation which did not spread over the whole region and also (2)  
307 to allow better comparison with previous works as Klein et al. (2015) and those that focused on  
308 onset like Sultan and Janicot (2000, 2003). The obtained rainfall distributions have been divided  
309 into three subsets according to the TRMM distribution which is considered as the reference here:  
310 the light rain when the rain value is below or equal to the 25<sup>th</sup> percentile of the TRMM distribution  
311 (3.46 mm/3hr), the medium rain with values between 25<sup>th</sup> and 75<sup>th</sup> (6.50 mm/3hr) percentiles, the  
312 intense rain events for values above or equal the 95<sup>th</sup> percentile (9.50 mm/3hr). It is worth noting  
313 that all the non-rain events have been beforehand removed in order to consider only the statistics  
314 based on effective rain events. Since the resolution of the dataset can impact the number of events,  
315 we computed these numbers using (1) the native grid of each dataset (solid line) and (2) the  
316 regridded datasets on the TRMM grid (dashed line).

317           Lighter rain events occur mostly between mid-night and 12 UTC (note that local time in  
318 JJA over this sub-region is close to time UTC) than during the second half of the day, with a  
319 maximum of occurrence at 12 UTC according to TRMM observation dataset. Both WRF, in their  
320 native grids, replicate the shape of the diurnal cycle of light rain events with a sudden decrease at  
321 12 UTC, but the occurrence of events is strongly overestimated in the parameterized run. If the  
322 explicit run capture well the timing of the maxima of the light rains, wrf-24km shows a 3-hours  
323 early peak of light rain events. On the other hand, wrf-4km either with its native grid or the  
324 regrided underestimates night lighter rain events. As of wrf-24km, the regrided data shows  
325 more lighter rain events than its native data.

326           In the range of medium rain events, the diurnal cycle is of less variation in TRMM even  
327 though a maximum is observed at 15 UTC and a minimum between 03 and 12 UTC. WRF-4km,  
328 in its native grid spacing, shows a more pronounced peak of the maxima of medium rain events  
329 and a wide rain events under the observation while its regrided product almost continuous less  
330 rain events related to the native wrf-4km. However, native and regrided grid from wrf-4km  
331 indicated the maxima of medium rain events at 15 UCT. Wrf-24km shows same pattern of diurnal  
332 cycles of the occurrence of the medium rain events either for the native and the regrided data.  
333 Nonetheless, a reduction in the number of rain events is noticed with the regrided product. All  
334 datasets agree on the timing of occurrence of minimum medium rainfall events in between 03 and  
335 12 UCT. Yet, wrf-24km displays the maximum events in the interval 15 and 18 UTC.

336           According to TRMM observation data set, intense rain events can occur anytime with  
337 nearly the same probability but none of the simulations reproduces this. The explicit run exhibits  
338 intense rain occurrence mainly from the evening to early morning with a maximum around 00  
339 UTC. The same timing of the diurnal cycle is retrieved with the regrided wrf-4km with more  
340 intense rain events.

341           The relative absence of intense rain events with wrf-24km is related to the lower value of  
342 the 95<sup>th</sup> percentile obtained by this convective parameterized run. The analysis of the occurrences  
343 of intense rain based on the 95<sup>th</sup> percentile of wrf-24km (figure not shown) demonstrates that this  
344 parameterized run mostly locates its maxima rain events in the afternoon (maximum at 15 UTC).  
345 This occurrence of maxima of intense rain events at 15 UTC with the parameterized run is mainly  
346 due to the fact that convection is generally high when net radiative energy is at its maximum at

347 about 15 UTC. The observed natural characteristics of rainfall are hardly replicated by models.  
348 This has been earlier highlighted in previous studies and suggested to be due to parameterisation  
349 of convection in the models (Marsham *et al.*, 2013, Dirmeyer *et al.*, 2012, Stephens *et al.*, 2010).  
350 Wrf-4km seems to produce maximum of rain independently to the peak of the net radiative energy,  
351 except for medium rain-rates. In term of diurnal mean amount and timing of rain events, wrf-4km  
352 depicts results closest to the observations in comparison to wrf-24km.

353 **Regriding WRF outputs into the grid scale of TRMM dataset has an effect on the number**  
354 **of the events regardless of the range of rainfall intensity, however, the timing is preserved.**

### 355 **3.3 Summary of the skill of the simulations on rainfall**

356 Figure 5 shows the daily Empirical Probability Distribution Functions and the boxplots of  
357 daily wrf-24km and wrf-4km precipitation compared to the ground-based observations, TRMM  
358 and CHIRPS data sets. Based on the available data and the regime of the rainy season, the area has  
359 been divided into two zones: the Guinean Coast (4°N-8°N and 10°W-10°E) and the Sahelian  
360 region including the near Sahel (10°N-18°N and 10°W-10°E). Only the available stations of each  
361 sub region are considered (CI1-7, BN1-3, GH2-5, GH7-8, GH12-62 for the Guinean Coast zone  
362 and GH1, GH6, GH9-11, BF1-7, NR1-7, GH40-44 for the Sahel region). For all datasets, the  
363 amount of precipitation at the nearest grid point of each station has been extracted. Following Lind  
364 *et al.* (2016), the PDF(fig.5, top) gives a detail on the spread/intensity of the daily rainfall for each  
365 of the dataset while the box plot (fig.5, bottom) for its part shows the summary of the distribution  
366 of rainfall (extremes, mean state). The percentiles on the box plots have been computed by  
367 considering only the wet days (the day where rainfall is above the threshold 1mm) over the period  
368 March-November. For each dataset, the number of events which overpass the 95<sup>th</sup> percentile of  
369 ground-based observations is also indicated. The numbers on the figure provides a clear view of  
370 the ability of the model to statistically replicate intense rain events. They indicate the occurrence  
371 of intense rain events with the specifics dataset.

372 Over the Guinean Coast area, there is a relative underestimation of the overall rainfall  
373 tendency by both TRMM and CHIRPS estimation compared to the ground-based observations.  
374 They show value generally below the ground-based observation(top). The box plots (summary)  
375 show only 2.95% of rain events for TRMM and CHIRPS as intense and also 95% of the rain

376 intensities are below 39 mm/day for TRMM and ~35mm/day for CHIRPS). There are marginal  
377 differences between both satellite-based dataset as the exhibit very close frequency occurrence  
378 pattern of rainfall and similar summary in both Guinean Coast area and Sahel. Across both sub-  
379 domain (Guinea Coast and Sahel), WRF-24km shows also less intense rain events as indicated  
380 with the PDF, the small boxes and the low value of its mean rainfall amount. In Guinea Coast,  
381 95% of the rain events are less than 21.78 mm/day and only 0.18% of the rain events are intense,  
382 while the ground-based observation shows the 95<sup>th</sup> percentile at 54.5 mm/day and a mean value of  
383 about 16.45 mm/day. The statistics displayed by the observations are well replicated by the wrf-  
384 4km, which shows 13.45 mm/day as mean value, and 4.66% of values are above the threshold of  
385 54.4 mm/day. Thus, the explicit convection run, despite its dry bias at seasonal scale along the  
386 Guinean coastal area during the Sahelian phase of the monsoon, replicates more realistic  
387 precipitation extremes and qualitative distributions compared to the convective parametrized  
388 convection run.

389 Over the Sahelian region, the explicit run shows daily rainfall frequency distribution closer  
390 to TRMM, CHIRPS and the ground-based observation. The summary provides more intense rain  
391 events where 95% of the rain are up to 52.31 mm/day and the simulation runs at 24km shows less  
392 intense rain events compared to the ground-based observation. 2.95% (wrf-24km) and 11.61%  
393 (wrf-4km) of rain events are above the threshold of 40 mm/day corresponding to 95<sup>th</sup> percentile of  
394 rainfall in the Sahelian region. The numbers of rain events based on wrf-4km are 4416 in the Gulf  
395 of Guinea; and 1499 in the Sahel. This matches better those of the observation with 3683 in the  
396 Gulf of Guinea; and 1119 in the Sahel than wrf-24km which shows 8250 in the Gulf of Guinea;  
397 and 2455 in the Sahel. Even though wrf-4km overestimates the number of intense rains and the  
398 intensity, it provides more realistic estimations precipitation extreme across both Guinea Coast  
399 and Sahel and emphasizes the benefit of the high-resolution simulation.

400 The low value of the occurrence of intense rain with wrf-24km compared to the high-  
401 resolution run may be explained by the difference of the size of the grid scale. With a coarser grid  
402 scale, there is a higher probability that sub grid scale rainfall events might not be captured. (Chen  
403 and Knutson 2008). Previous studies (Emori et al. 2005; Iorio et al. 2004; Kharin et al. 2005) which  
404 assessed climate models by using ground-based stations data concludes that it is not a simple task  
405 to make a comparison between model output and station data set. They also reported that rainfall

406 extreme indices might be influenced by the model resolution. The station records are essentially  
407 point estimates while the model output represents the rainfall variability over a wider spatial scales.  
408 Chen and Knutson (2008) also argued that Regional climate models are able to dynamically  
409 downscale extreme precipitation events to a spatial scale that is more comparable with observed  
410 rainfall analysis or station data. The grid scaling issues should be then reduced. Furthermore, even  
411 though it is not easy to cut off the physics from the pure resolution effect behind the differences  
412 between the runs at 24km and 4km, it nevertheless emphasizes the usefulness of running the model  
413 at higher resolution at least to focus on the extreme events. **On the other hand, both rainfall from  
414 wrf-24km and wrf-4km have been upscaled to TRMM dataset grid scale to assess the impact of  
415 the downscaling effect in the differences between those two (2) WRF outputs. Similar analysis as  
416 figure 5 has been made with the reggrided data and the results (figure not shown) indicated  
417 marginal changes between the native and reggrided rainfall. For example, the comparison of the  
418 value of the 95<sup>th</sup> percentile with native and reggrided shows is a reduction of about 7.41% (Gulf  
419 of Guinea) and 5.3% (Sahel) for wrf-24km while wrf-4km indicates a decrease of 7% (Gulf of  
420 Guinea) and 2.5% (Sahel). This result may suggest a combination of both grid scale factors and  
421 physics on the observed differences between the runs at 24km (parameterized convection) and  
422 4km (convection-permitting).**

#### 423 **4. Dynamical and physical role of the West African Monsoon**

##### 424 **4.1 Dynamics of the monsoon and moisture flux**

425 The link between the dynamics of the WAM and its associated rainfall has been variously  
426 investigated and emphasized the role of the atmospheric circulation and specifically the Moisture  
427 Flux Convergence (MFC) (Cook, 1999; Druyan et al., 2010 ; Fontaine et al., 2008 ; Fontaine &  
428 Philippon, 2000 ; Lebel et al., 2003 ; Nicholson, 2008, 2009, 2013 ; Nicholson et al., 2012 ; Sylla  
429 et al., 2010).

430 Figures 6 shows cross sections of the zonal wind from March-May (MAM), June-August  
431 (JJA) and September-November (SON) and averaged from 10°W to 10°E. The first column  
432 represents the seasonal mean, while the second and third columns represent respectively the  
433 seasonal mean bias of wrf-4km and wrf-24km related to Era-Interim. Figure 7 shows seasonal

434 mean of vertical profiles of the MFC, superimposed by the meridional-vertical wind vectors (v,w).  
435 For a better comparison, all data have been interpolated to the wrf-24km dataset.

436 The atmospheric circulations related to the WAM, characterized by the monsoon flow, the  
437 African Easterly Jet (AEJ) and the Tropical Easterly Jet (TEJ) are clearly replicated by the model  
438 outputs.

439 During spring (MAM), the core of the monsoon flow as shown by ERA-interim is  $\sim 4\text{m}\cdot\text{s}^{-1}$   
440 while WRF is showing higher monsoon flow toward the coast (wrf-24km: up to 5m/s and wrf-4km  
441 up to 3m/s) and lower flow in the north (up to 4m/s below for both wrf-24km and wrf-4km) (Fig.  
442 6). Deep convection, associated with strong updrafts corresponding to the ascending branch of the  
443 Hadley cell, occurs between  $6^{\circ}\text{N}$  to  $10^{\circ}\text{N}$  and 800 hPa to 200 hPa. This feature is well reproduced  
444 by the model outputs either wrf-24km or wrf-4km (Fig. 7).

445 During the summer (JJA), ERA-interim shows two distinguished cores of the monsoon flow.  
446 The major one is located around  $15^{\circ}\text{N}$  and the minor one at roughly  $5^{\circ}\text{N}$ . Wrf-4km reproduces  
447 these two cores; however, the cores have the same intensity, the southern one is located further  
448 north than for ERA-interim, around  $7.5^{\circ}\text{N}$ , while the second one is around  $13^{\circ}\text{N}$  (figure not  
449 shown). The AEJ is stronger in ERA-interim than in WRF simulations, while TEJ is weaker  
450 (Fig.6). Wrf-4km is showing difference up to 1m/s while wrf-24km reaches 2m/s in term of AEJ.  
451 Both WRF output show similar replication of TEJ (up to 2m/s lower). As expected, the area of  
452 deep convection has now moved to more northerly position from its position during the spring  
453 (MAM). Both model outputs replicate this feature with more inland penetration (up to 15N) than  
454 Era- Interim (below 13N and less pronounced (Fig. 7). This inland location of the deep convection  
455 is also coherent with the distribution of rainfall with WRF. A subsidence is observed around  $5^{\circ}\text{N}$   
456 with wrf-24km and wrf-4km while in ERA-interim, it is located further beyond the equator (around  
457  $2^{\circ}\text{S}$ ). All these differences are coherent with the more southward position of the maximum of  
458 rainfall in ERA-interim (Figs. 2 and 3) and explain the dry bias of ERA-interim over Sahel which

459 is consistent with stronger AEJ and weaker TEJ ((Omotosho 2008)) and the dry bias of WRF above  
460 the sea. Indeed, the subsidence at 5°N generates a zone of strong divergence around the coastline  
461 (1000-800 hPa, 2°N-8°N) in the simulation, which is weaker and more to the south in ERA-  
462 interim. Note also that just above this layer, a layer of weak convergence around 700 hPa is  
463 simulated with northerly wind and likely corresponds to the low-level shallow circulation (LLSC)  
464 induced by the Saharan heat low and discussed by (Zhang et al. 2006). This LLSC is not captured  
465 by the reanalysis.

466 During fall (SON), the configuration is similar to the spring one with less intensity. The  
467 southwesterly monsoon flow is confined southwards of 5°N with Era-Interim and stronger in WRF  
468 with more inland penetration. Wrf-24km shows more intense monsoon flow with a bias up to 4-  
469 5m/s and the explicit run shows bias below 3m/s relative to Era-Interim.

470 To conclude on the dynamics at seasonal and regional scales, several features can explain the  
471 differences in the seasonal precipitation patterns between ERA-interim and WRF simulations,  
472 despite the spectral nudging. This result reveals more or less important interactions between scales  
473 over this area and an impact of regional/local processes in the dynamics of this region. Therefore,  
474 the impact of physical processes seems not negligible in the representation of all elements of the  
475 WAM. The differences between the two WRF domains, which share the same physics but not  
476 convection, are mainly reduced to the low-level circulation, which has a stronger zonal component  
477 in WRF-24km than in WRF-4km. It affects the intensity of moisture convergence between 5 and  
478 10°N. Furthermore, wrf-4km shows less deviation from Era-Interim than wrf-24km in the  
479 replication of the main features of the WAM. However, these differences generally less  
480 pronounced or even marginal. Next section investigates the impact of physical processes by  
481 performing several simulations with different physics using the same large scale forcing.

## 482 4.2 Impact of physical processes

483

484 One of the major challenge of the current Convection-Permitting Models (CPMs) are the fact  
485 that they are still relying in older and traditional approach parametrization developed for

486 boundary layer turbulent in mesoscale models. Furthermore, they are running at grid spacing that  
487 are not large enough to be in mesoscale model regime nor fine enough to be fallen into large-  
488 scale eddy simulation regime as discussing in Tao and Moncrieff (2009)

#### 489 4.2.1 Sensitivity of WRF parametrizations on precipitation over the southern coastal area 490

491 The aim in this section is to identify configurations that would be suitable for a better  
492 representation of intense rain events over the Guinean coast area. The past conducted works like  
493 Flaounas et al. (2011); Pohl et al. (2011); Klein et al. (2015), used parameterized convection. Prein  
494 et al. (2015) in a review CPMs underlined the limitation of our understanding about the  
495 microphysical processes and their interaction with resolved cumulus dynamics while Tao and  
496 Moncrieff (2009) indicated the grid spacing issue in the representation of boundary layer turbulent.

497 The current work focuses on the sensitivity of microphysics and PBLs to the resolved cumulus and  
498 contribute to the understanding of the microphysics processes and their interaction with resolved  
499 cumulus dynamics. Even though, the change of the convection scheme may modify the results,  
500 this will need too much resources and beyond the scope of this paper.

501 A second set of experiments has thus been performed but with smaller domains due to  
502 computing resources. The inner domain has been reduced to the Guinean coast area extending  
503 from the **Ivory Coast** to the Republic of Benin (Figure 1, pink rectangles). The period of the  
504 experiment is June 2014 when many flood events have been recorded along the littoral of the Gulf  
505 of Guinea and especially in Abidjan. The following different experiments use the configuration of  
506 the first set except for the microphysics (MP) and planetary boundary layer (PBL) schemes, which  
507 contribute to the vertical and horizontal distributions of moisture, which is a key issue in the  
508 Tropics for rainfall processes ((Neelin et al. 2009); (Holloway and Neelin 2009)). Nine  
509 combinations of MP\_PBL have been tested, using 3 different PBL schemes and 3 different MP  
510 schemes. These 9 combinations are thus associated with the Kain-Fritsch convective scheme in  
511 the coarser domain and with explicit convection in the inner domain. Since these parameterizations  
512 manage the atmospheric moisture distribution based on the same large-scale information provided  
513 by same lateral boundary conditions and the use of spectral nudging for wind and temperature, this  
514 protocol is well suited to understand the role of the physical processes in the simulated rainfall  
515 estimate over this specific area.

516 The role of the PBL scheme is to determine the flux profiles of temperature and moisture within  
517 the whole atmospheric column, hence generating tendencies that serve as input for the CU and MP  
518 schemes at every model time step. Two types of PBL schemes exist according to the way they  
519 approach the turbulence equation closure problem: local closure schemes and non-local closure  
520 schemes. In the local closure schemes approach, the turbulence fluxes at each grid point are  
521 estimated based on prognostic turbulence kinetic energy (TKE). The Mellor–Yamada–Janjic  
522 (MYJ: (Janjic 1994; Janjić 2002) boundary-layer scheme used in the first part of this paper is of  
523 this type. The non-local closure schemes consider that scale eddies are of major importance to  
524 estimate vertical mixing in the boundary layer and in the free atmosphere. The PBL YonSei  
525 University (YSU: (Hong et al. 2006)) and the Asymmetric Convective Model version 2 (ACM2:  
526 (Pleim 2007) used in this section are based on this non-local closure. Moreover, the ACM2 is a  
527 combination of local and non-local turbulence closure techniques (Xie et al. 2012).

528 The microphysics scheme includes all processes that control the formation of cloud  
529 droplets and ice crystals, from their growth to their fallout as precipitation. It includes explicitly-  
530 resolved water vapour, cloud and precipitation processes. The MP scheme is in charge to remove  
531 excess atmospheric moisture in case the air is still saturated, which we will refer to us as non-  
532 convective precipitation. The different MP schemes used are based on their classification of hydro-  
533 meteors. The size distributions can differ from one scheme to another. The schemes considered in  
534 this work are the single-moment six-class (WSM6) scheme (Hong and Lim, 2006), the double-  
535 moment Morrison (MOR) scheme (ten-class) (Morrison et al. 2009) and the New Thompson (TH)  
536 scheme (Thompson et al. 2008). Table 1 provides a summary of the schemes used and the different  
537 experiments.

538 Here attention is mostly given to the qualitative impact on rainfall over Guinean coast area.  
539 Figure 8 displays Empirical probability distribution functions of daily precipitation (top) which  
540 provides the frequency occurrence of the rain events according to the intensity and the daily  
541 boxplots of precipitation. These have been computed for wrf-24km and wrf-4km rainfall from each  
542 ensemble group members, TRMM and CHIRPS dataset across Guinea Coast area. The groups  
543 have been built using a fixed particular scheme following (Pohl et al. 2011). Thus, each ensemble  
544 group is the mean of all the configurations which use that particular scheme. The value of the  
545 rainfall is extracted at the nearest grid point of each station from the different run outputs, TRMM

546 and CHIRPS. A single time series is computed for each data set. From these time series, we  
547 removed the days when observations are lacking and the dry days (where daily rainfall is below 1  
548 mm/day). The result indicates significant underestimation of the overall rainfall intensity of wrf-  
549 20km compared to TRMM, CHIRPS and ground-based observation as seen it with the low  
550 frequency occurrence of rain events against the intensity. Wrf-4km for its part is able to retrieve a  
551 good range of the rain events in regard to the intensity. CHIRPS dataset is showing statistics closer  
552 to the observed ground-based data compare to TRMM which miss more rain events. The boxplot  
553 of observations is then obtained from the total number of precipitating days of all stations of the  
554 Guinean area (CI1-7; BN1-3, GH2-5, GH7-8, GH12-62), i.e. 586 samplings (see Tab. 2). The same  
555 for TRMM and CHIRPS for which we obtained 656 and 553 samplings respectively. For the  
556 simulations, the numbers of the rain events are relatively high (see Tab. 2), with lower values at  
557 4km than at 20km partly due to the effect of resolution, as already explained in the previous  
558 section.

559         In the month of June during which several flooding events were reported, 11.43% of events  
560 above the threshold of 54.5 mm/day were recorded. All the ensemble members show less intense  
561 rain events compare to the ground-based observation and TRMM data sets. In addition, the total  
562 rainfall amount was also underestimated by all the ensemble members (not shown). However,  
563 clearly, the main impact comes from the use of higher resolution since the mean, max, 3<sup>rd</sup>  
564 interquartile and number of extreme events are always significantly higher in WRF-4km than in  
565 WRF-20km ensembles.

566         The occurrence of intense rain events is about 4.21% with the ensemble with the PBL  
567 scheme ACM2 which provides the closest statistics to TRMM data set, at 4km while with WRF-  
568 20km run, all the ensembles do not reach at once the value of 54.5 mm/day or have an occurrence  
569 below 0.3%. However, it is biased by the fact that the comparison with local rain gauges is better  
570 suited to a run at 4-km resolution than at 20km resolution. Nevertheless, it appears that physics  
571 also impacts the results. All statistics are in better agreement with observations than the others set  
572 of runs at a similar resolution (i.e. 1<sup>st</sup>, 2<sup>nd</sup> and 3<sup>rd</sup> quartiles, mean, max and 95<sup>th</sup> percentile). It is  
573 true for the domain at 20km and the one at 4-km. Two other ensembles at 4km outperform the  
574 others, not for all statistics but for the value of the 95<sup>th</sup> percentile of precipitation and 3<sup>rd</sup> quartile,

575 which indicates a better ability to produce heavy rain: the ensemble using WSM6 as MP scheme  
576 and the one using YSU as PBL scheme.

577 The same box plot was also performed over the Guinean Coast region (4N-8N; 10W-5E) for  
578 WRF simulations and TRMM by using the same grid as TRMM before statistics are computed  
579 (figure not shown). The result raised once again the better performance of the explicit convection  
580 in the statistics of the rainfall distribution (moderate, intense and extreme rainfalls). This suggests  
581 that the added value of the explicit run did not only come from the resolution but also from explicit  
582 convection. It further emphasizes the usefulness of convection permitting in the analysis of  
583 extreme rainfall and more general extreme events. However, convection permitting with high-  
584 resolution run, is yet exhaustively enough to fully address the problem of simulating of rainfall  
585 over West African region and especially over the Guinean Coast and surrounding.

586

#### 587 4.2.2 Impact of PBL scheme

588 Both PBLs schemes ACM2 and YSU are non-local closure schemes which gives more  
589 attention to scale eddies on the estimation of vertical mixing in the boundary layer and the free  
590 atmosphere. The MYJ, which is a local closure, displays less intense rain events. The better  
591 performance of non-local closure schemes compared to the local one has been previously reported  
592 (Pleim 2007). The non-local closure has a better ability to replicate the turbulent vertical transport  
593 when both small-scale shear-driven turbulence and large-scale convective turbulence are taken  
594 into account (Holtslag and Boville 1993). This also takes into account large eddy transport and  
595 entrainment effects, which is essential for realistic representation of the convective boundary layer  
596 and the transport of humidity from the surface to the lower free troposphere, which is key for  
597 triggering of convection (Holloway and Neelin 2009). The difference of vertical profiles of  
598 humidity between the six PBL sub-ensembles is shown in Fig. 9 and clearly reveals that stronger  
599 differences appear between 925 and 750 hPa than close to the surface, and the moister this layer,  
600 the heavier the precipitation. These differences, however, are more noticeable with wrf-20km than  
601 with wrf-4km. This may suggest a less influence of the PBL scheme on the convective permitting  
602 run.

603 The latitudinal evolutions of surface conditions are analysed via the latitudinal profile of  
604 2-meter temperature (T2m), 2-meter specific humidity (Q2m), downward shortwave (SW) and  
605 longwave (LW) radiation fluxes (Fig. 11). The analysis reveals 2 distinctive groups over the  
606 Guinean Coast for T2m, Q2m, and LW, between the wrf-20km and wrf-4km. The explicit runs  
607 show higher surface temperature, more humidity and more incoming longwave radiation fluxes. It  
608 is also worth noting that there are important differences in the near surface humidity north of 8N.  
609 While wrf-4k runs show decrease in the humidity towards the north, wrf-20km runs show an  
610 increase. Important differences are also observed between the PBL ACM2 and MYJ for simulation  
611 of T2m and Q2m in wrf-24km or wrf-4km runs. ACM2 PBL is warmer and drier at the surface  
612 than MYJ, while the opposite is observed in the free troposphere (Fig. 10). An important difference  
613 is also observed for SW but only with wrf-20km. Over the ocean, and near the coast, the spread  
614 between the sub-ensembles is strong with both wrf-20km and wrf-4km. These differences over the  
615 ocean likely strongly impact the humidity advection inland. Wrf-20km shows more LW with  
616 ACM2 with less SW. This implies a deeper or more persistent cloud cover, despite the fact that it  
617 is drier and relatively warmer on the surface. At wrf-4km runs however, there are less differences  
618 between the value of SW and LW. Generally, wrf-20km simulates more SW arriving at the surface  
619 than wrf-4km and vice versa for the LW.

#### 620 4.2.3 Impact of MP scheme

621 The MP scheme is not a strong discriminant for the atmospheric specific humidity either with wrf-  
622 20km and wrf-4km (Fig. 8). This is also true for T2m and Q2m (Fig 9). On the contrary, there are  
623 high differences between WSM6 and MOR in the representation of the SW with wrf-4km and  
624 slightly less with wrf-20km (Fig.10), and this may likely explain the differences in the rainfall  
625 distribution. The vertical profiles of occurrence (%) of the Liquid Water Content (LWC) and the  
626 Ice Water Content (**IWC, not shown**) are displayed for different bin categories in Fig. 11  
627 respectively. Figure 11 shows that LWC is sensitive to the resolution more than to the MP scheme  
628 used, since distributions are very similar between different MP ensembles, but very different  
629 between WRF-20km and WRF-4km. At 4km, there is higher occurrence of strong values of LWC  
630 between 925 and 750 hPa, consistent with higher specific humidity at this altitude. It impacts more  
631 strongly LW than SW, meaning that these clouds likely appear during nighttime. For IWC,  
632 differences between different MP schemes are stronger than between the two different resolutions

633 (not shown). However, the main difference exists between TH and other schemes, while the  
634 difference between MOR and WSM6 is weak. It thus cannot explain the difference of SW obtained  
635 between MOR and WSM6.

636

## 637 5. Conclusions

638 This work focuses on the sensitivity of the Weather Research and Forecasting (WRF)  
639 Model to horizontal resolution and physics schemes in the replication of West African precipitation  
640 for the year 2014. Several runs were performed with either parameterization or explicit convection.  
641 Both runs, wrf-24km and wrf-4km, at seasonal scale, are able to replicate rainfall distribution over  
642 the region. The high-resolution which uses the explicit convection exhibits driest bias along the  
643 coast of the Gulf of Guinea but generally outperforms the 24km run especially in the replication  
644 of the extreme rainfall distribution. The feature underlines the importance of high resolution on  
645 the analysis, characterization and further forecast of extreme events. At diurnal scale, based on  
646 TRMM data set, the major light rain events occur between mid-night and 12 UTC and the diurnal  
647 cycle of medium rain events has of less variation with a maximum observed at 15 UTC. Wrf-4km  
648 outperforms wrf-24km in the replication of these features especially the timing, and the number of  
649 events. Intense rain events can occur anytime with nearly the same probability but none of the  
650 simulations reproduces this. The parametrized convection run situated this maximum of  
651 occurrence of intense rain events in the afternoon at 15 UTC. This is mainly due to the fact that  
652 convection is generally high when net radiative energy is at its maximum, near 15 UTC for these  
653 regions. This has been earlier highlighted in previous studies and suggested to be intrinsic to  
654 parameterized convection (Marsham *et al.*, 2013, Dirmeyer *et al.*, 2012, Stephens *et al.*, 2010).  
655 Furthermore, the explicit run exhibits intense rain mainly from the evening to early morning with  
656 a maximum around 00 UTC, independently to the peak of the net radiative energy. In short, the  
657 observed typical diurnal distribution of the rain is hardly well simulated by the model.

658 The analysis also reveals an adequate representation of the dynamical features of West  
659 African monsoon system with a less subsequent added value of permitting convection in the  
660 replication of low levels atmospheric circulation. However, irrespective to the spectral nudging  
661 for wrf-24km towards ERA-interim, there are differences of the dynamical structures between  
662 ERA-interim and wrf-24km. This reveals important interactions between scales over this area and  
663 not negligible impact of regional/local processes on the dynamics of this region. Therefore, the  
664 impact of physical processes seems crucial in the representation of all elements of the WAM. Both  
665 wrf-24km and wrf-4km well replicate the seasonal evolution of the AEJ. However, they show

666 stronger monsoon flow and weaker AEJ compared to ERA-interim. The strong AEJ leads to  
667 inhibition of the vertical ascent of moisture in ERA-interim; thus, less development of clouds. The  
668 relative low value of the AEJ displayed with WRF allows the vertical ascent of the moisture  
669 leading to more frequent clouds. This is in agreement with the high value of precipitation observed  
670 with WRF simulations inland. On the contrary, there is a dry bias over the Gulf of Guinea and  
671 surroundings seaboard (from 8°N and equatorward) with either parameterized and explicit  
672 convections. This dry bias has been associated with a more northward location of the subsidence  
673 branch of the Hadley cell and a less south-north spread of the rain belt observed in WRF outputs.  
674 The differences between the two WRF runs, which share the same physics but not convection, are  
675 mainly reduced to the low-layer monsoon flow in JJA, which has a stronger zonal component in  
676 WRF-24km than in WRF-4km. It affects the intensity of moisture convergence between 5°N and  
677 10°N.

678 The impact of microphysics is not as strong as that of PBL schemes in either explicit or  
679 parametrized convection modes. However, some differences exist that can help in a better  
680 reproduction of heavy rainfall. Note that only complex MP schemes have been tested here, and it  
681 is possible that the use of more simple schemes may lead to different conclusions on the importance  
682 of MP scheme. The use of a non-local PBL scheme seems critical to better transport the low-layer  
683 humidity into the free troposphere and trigger convection.

684 The convection-permitting simulations thus seem well relevant to study extreme events  
685 (i.e. heavy precipitation). However, the simulations can be affected by the limitation of the domain  
686 size, the absence of two-way interactions between the inner domain and the rest of the globe, and  
687 the lateral boundary condition issues. Thus it is still ambiguous whether RCMs actually improve  
688 or degrade the larger scales information which is still a backbone for modeller and scientific  
689 community in general as underlined by Laprise *et al.* (2008).

690 The upscaling of wrf-4km to TRMM grid spacing (e.g. fig.4,6 and 7) suggested that  
691 differences may not be only related to grid spacing differences but a combination of both  
692 physical processes and grid scale effects. This study also indicates that the grid scale impact  
693 seems to be more pronounced at diurnal scale than daily and seasonal scales. In addition, as  
694 suggested by Prein et al. (2015) and Tao and Moncrieff (2009), the simulation at higher  
695 resolution bring out a key problem: the CPMs are still relying in the older and traditional

696 approach parameterization developed for boundary layer turbulence in mesoscale models. In the  
697 other hand, the current grid spacing of CPMS are not fine enough be into eddy simulation regime  
698 nor coarser to be consider as mesoscale models. This problem of upscaling is of paramount  
699 importance and need to be addressed however, this is beyond the scope of the current work.

700         The current study focuses only on a specific year due to the coast of such experiment. It  
701 is then important to extend to several years to allow better assessment of physical processes and  
702 statistical analyses. Such work needs subsequent cluster resources and is beyond the scope of this  
703 paper. The use of only three (3) microphysics and PBL and one convective parameterization  
704 scheme may be a limitation of the methodology.

705         This work is a first step in performing a set of comparison of different configuration that  
706 use various microphysics, PBL schemes and permitting convection. The current study justifies a  
707 need for large project work which will focus on the interaction between convection resolving and  
708 microphysics and PBLs schemes etc. It will contribute to better assess the skill of WRF in the  
709 replication of regional and more local physical processes. Furthermore, in order to fully isolate  
710 the changes related to the permitting convection from the pure grid scale impact (resolution) one  
711 may need a set of experiments using explicit and parameterized convections both carried at the  
712 same resolution. These are in the perspective of the Ivorian new computer center which will  
713 allow such expensive experiments.

714

715

716 **List of Tables**

717 Table 1: Cumulus, microphysics and planetary boundary layer schemes used for the experiments

718

	<b>PHYSICAL OPTION</b>	<b>REFERENCES</b>
<b>CUMULUS</b>	Kain–Fritsch (KF)	(Alapaty et al. 2012)
	Morrison double-moment (MOR)	(Morrison et al. 2009)
	New Thompson (TH)	(Thompson et al. 2008)
<b>MICROPHYSICS</b>	WRF Single-Moment 6-class (WSM6)	Hong and Lim 2006
	Asymmetric Convective Model V2 (ACM2)	(Pleim 2007)
	Mellor-Yamada-Janjic (MYJ)	(Janjic 1994)
<b>PLANETARY BOUNDARY LAYER</b>	Yonsei University (YSU)	(Hong et al. 2006)

719

720

721 Table 2: Total number of rainy events over 1410 possible.

Data set	number of rain events
Observation	586
WRF_ens_acm2_20km	1312
WRF_ens_acm2_4km	665
WRF_ens_myj_20km	1238
WRF_ens_myj_4km	1001

WRF_ens_ysu_20km	1323
WRF_ens_ysu_4km	992
WRF_ens_mor_20km	1255
WRF_ens_mor_4km	938
WRF_ens_th_20km	1340
WRF_ens_th_4km	878
WRF_ens_wsm6_20km	1321
WRF_ens_wsm6_4km	1025
WRF_ens_20km	1353
WRF_ens_4km	1070
TRMM	656
CHIRPS	553

722

723

724

725

726

727

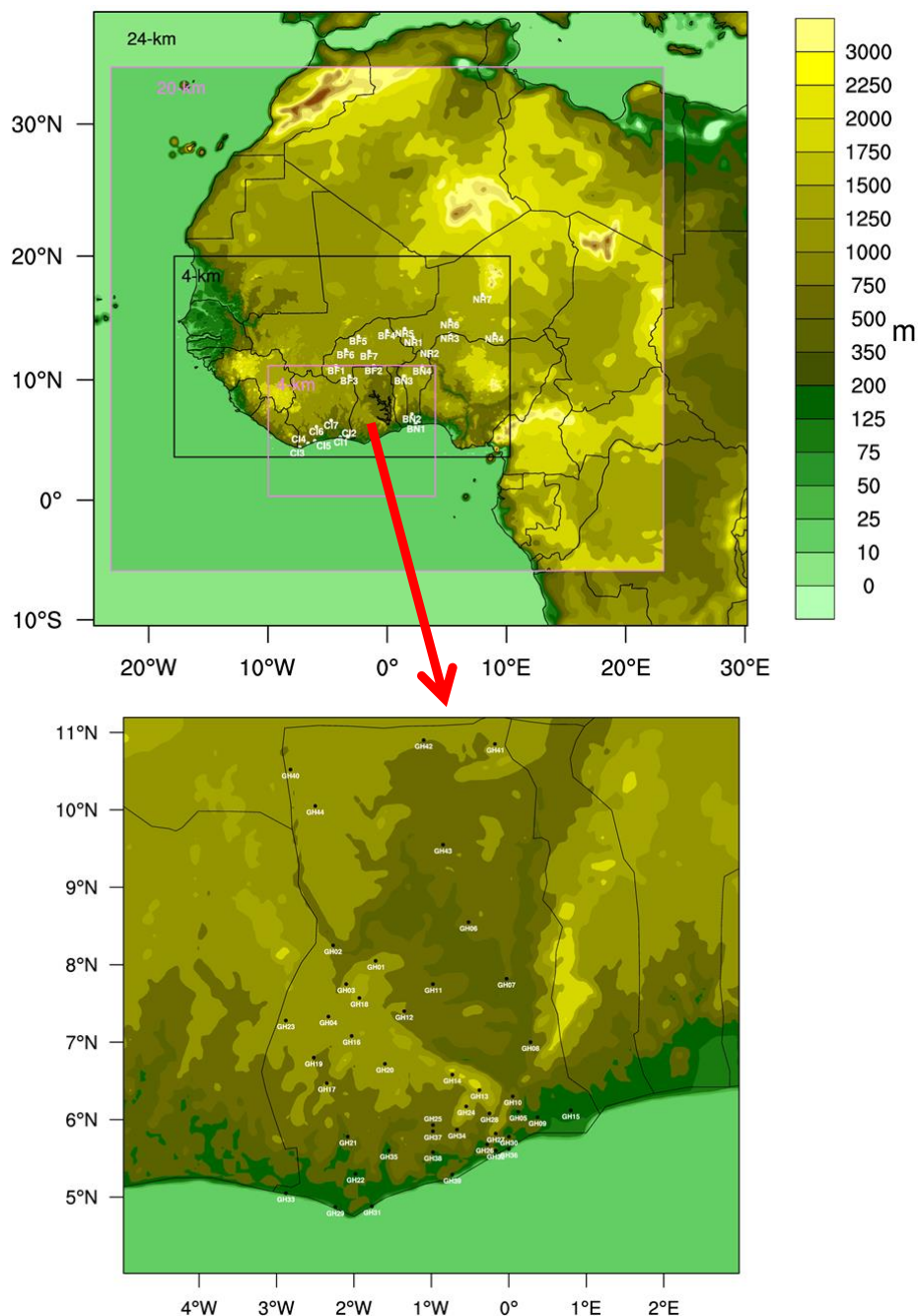


**Fig. 1** Top: WRF model domain and elevation (m); parent domain at 24 km horizontal resolution (25°W–30°E,10°S–40°N). The nested domain is depicted by the back box (17°W–10°E,4°N–20°N) black boxes (first set of runs). The pink boxes correspond to the domains for the second set of runs (sensitivity to MP and PBL schemes) where parent domain is at 20 km horizontal resolution (25°W–30°E,10°S–40°N). The nested domain covers the southern coastal area (10°W–5°E,0°N–12°N). The white dots indicate the ground-based stations used. Bottom: Zoom over Ghana (Table 1 provides the name and coordinates of the stations cited in the manuscript)

729

730

731

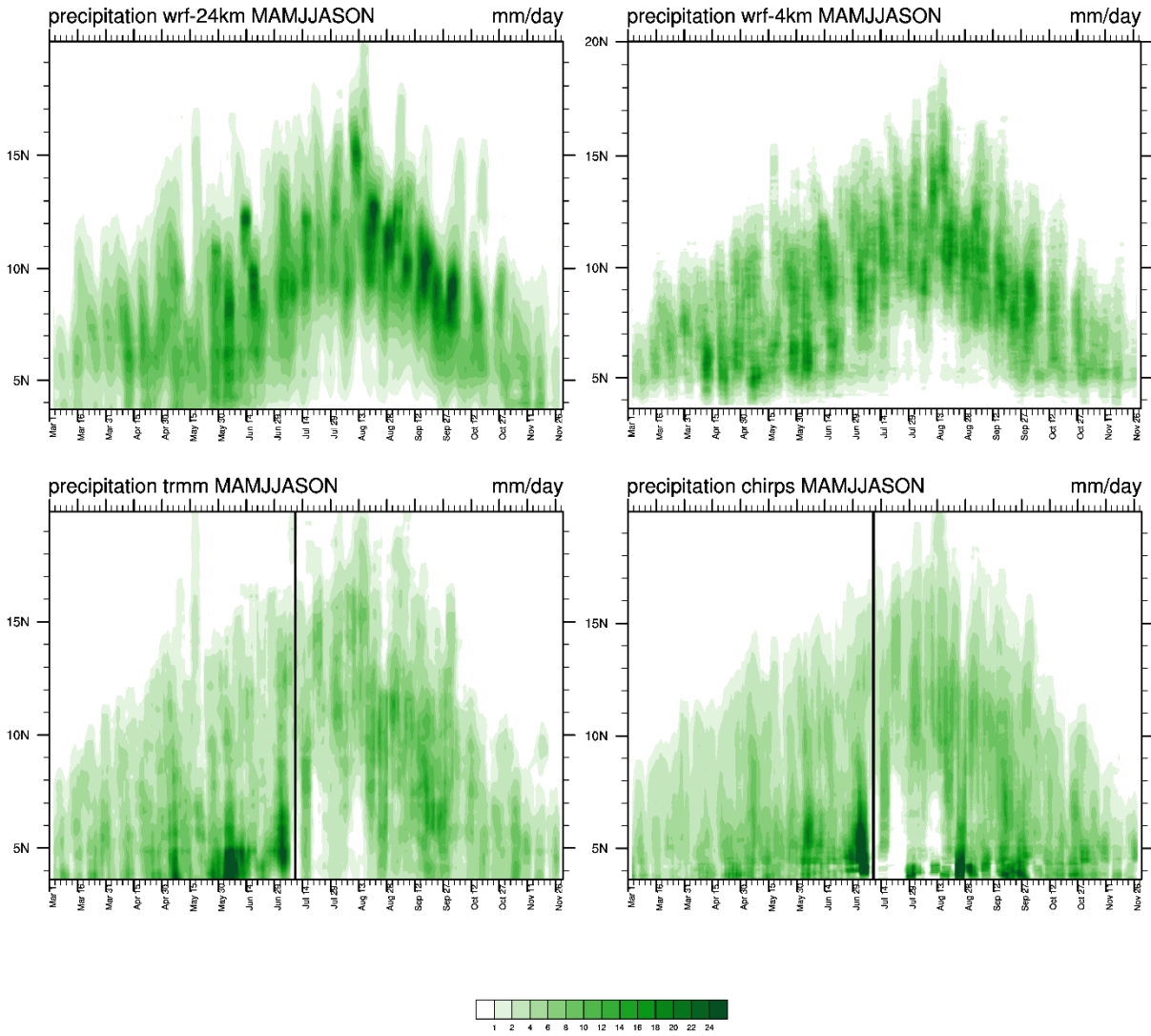


**Fig. 2** Seasonal evolution (time vs. latitude) of 5-day mean precipitation averaged between 10°W-10°E

732

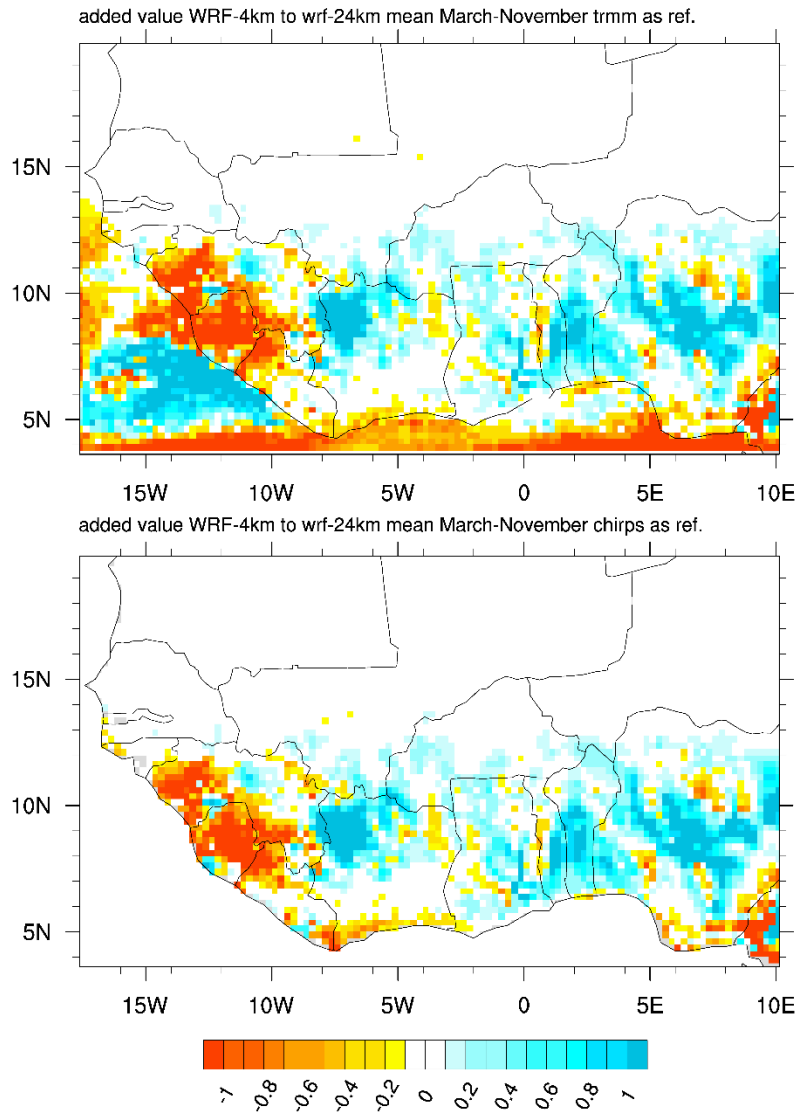


**Fig. 3** Added value of high resolution (wrf-4km) simulation to coarse resolution (wrf-24km): on top computed using TRMM as reference dataset and the bottom computed using CHIRPS dataset as the reference.

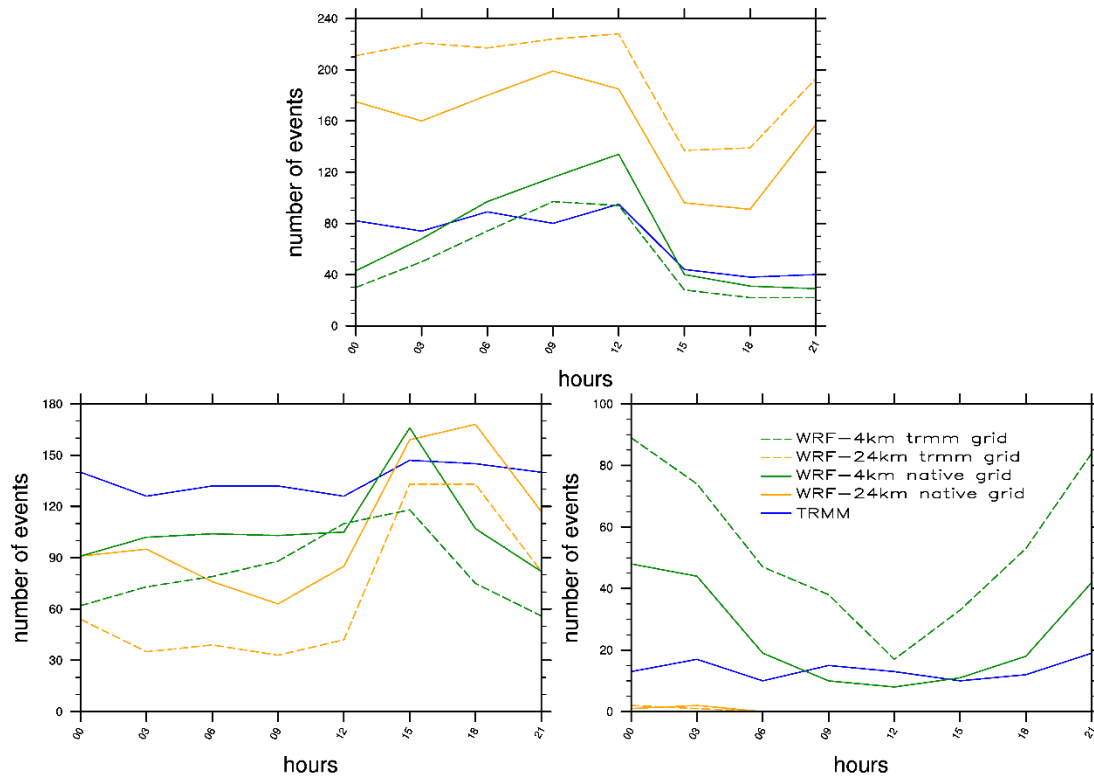


**Fig. 4** Diurnal cycle of rainfall occurrence according to the range of intensity computed from TRMM distribution (light, medium, intense); from TRMM (blue), wrf-24km (orange) and wrf-4km (green), averaged over Gulf of Guinea (4°N to 8°N and 10°W to 10°E). The dotted lines account for WRF regridded into TRMM coordinates and the full lines for WRF outputs on native coordinates. **Top panel shows light rainfall events; bottom-left and bottom-right present respectively the mediums and intense rainfall events.**

734

735

736

737

738

739

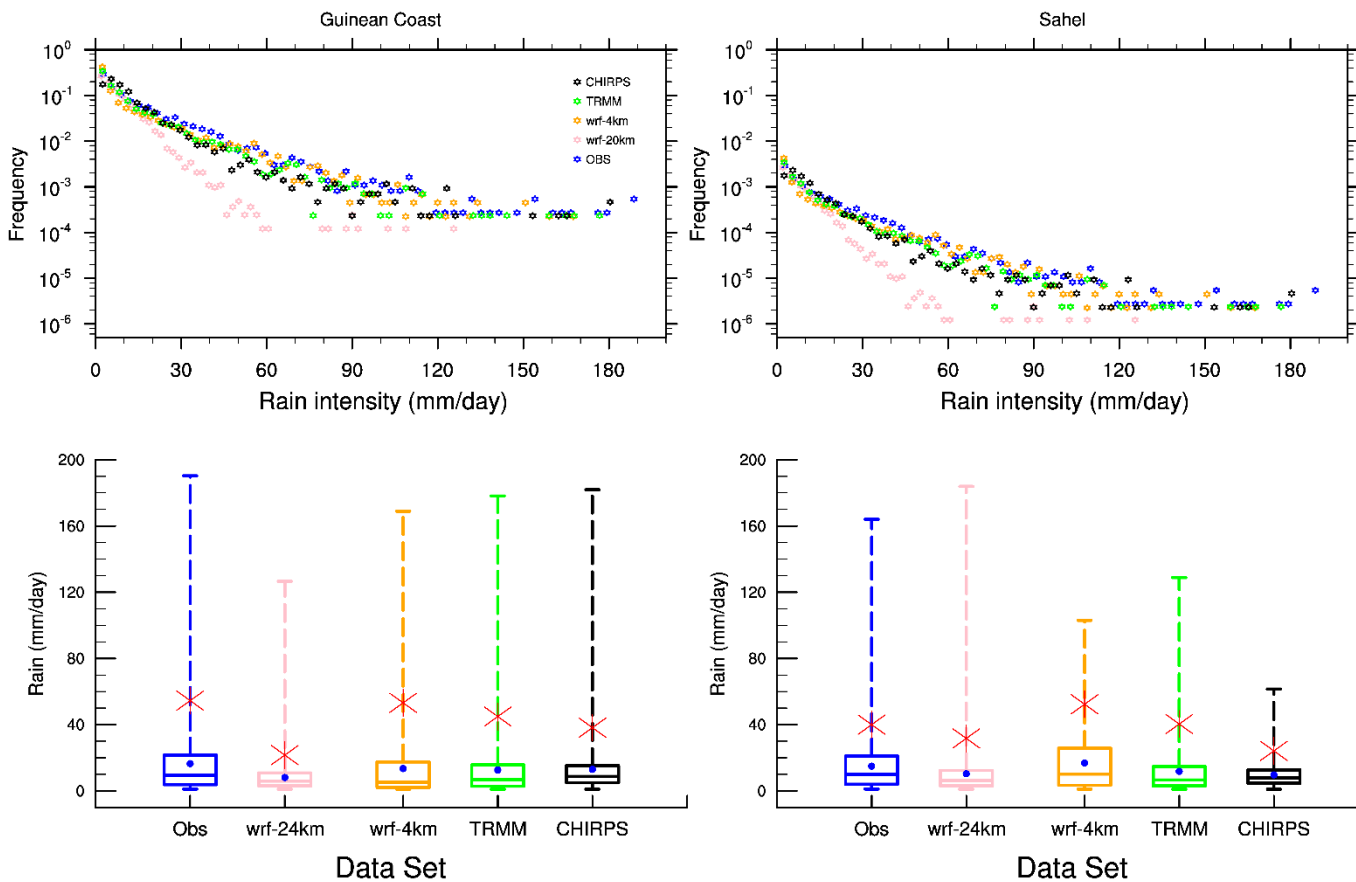


**Fig. 5** Empirical probability distribution functions of daily precipitation (top) daily. Boxplots of the daily precipitation (Bottom) respectively from the ground-based observations, wrf-24km, wrf-4km, TRMM and CHIRPS data sets over the Guinean coast (left) and the Sahelian (right) regions. The boxes indicate respectively from the bottom to the top the first, second and third interquartile ranges and the whiskers stretch to minimum and maximum values of each data set. Blue dots and the red stars represent respectively the mean value and the 95<sup>th</sup> percentile of the precipitation for each data set.

740

741

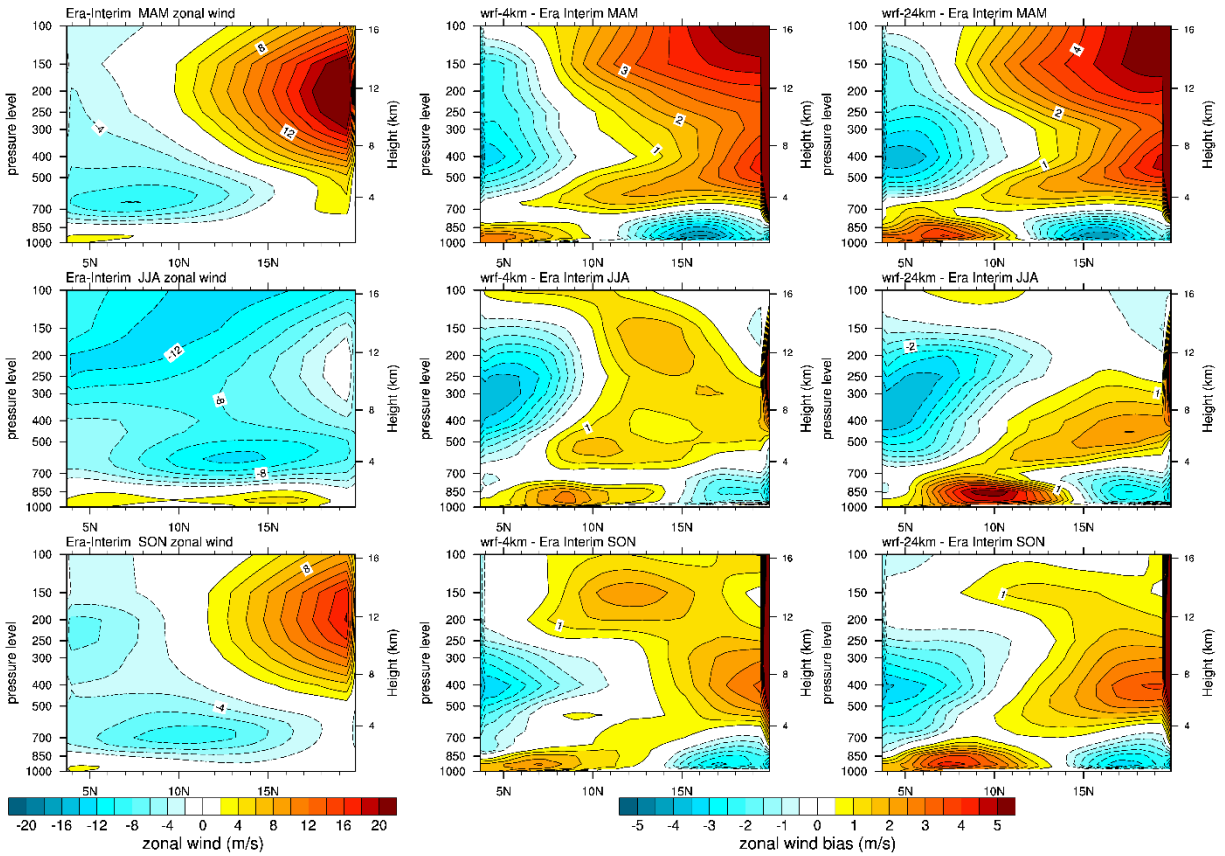


**Fig. 6** Seasonal mean cross sections of the zonal wind from March-May, June-August and September-November and averaged from 10°W to 10°E. Column 1 represents ERA-interim; column 2 and column 3 represents respectively the difference between ERA-Interim, wrf-4km and wrf-24km. Dashed contours and blue colours stand for negative values and solid contours and red colours are for positive values.

742

743

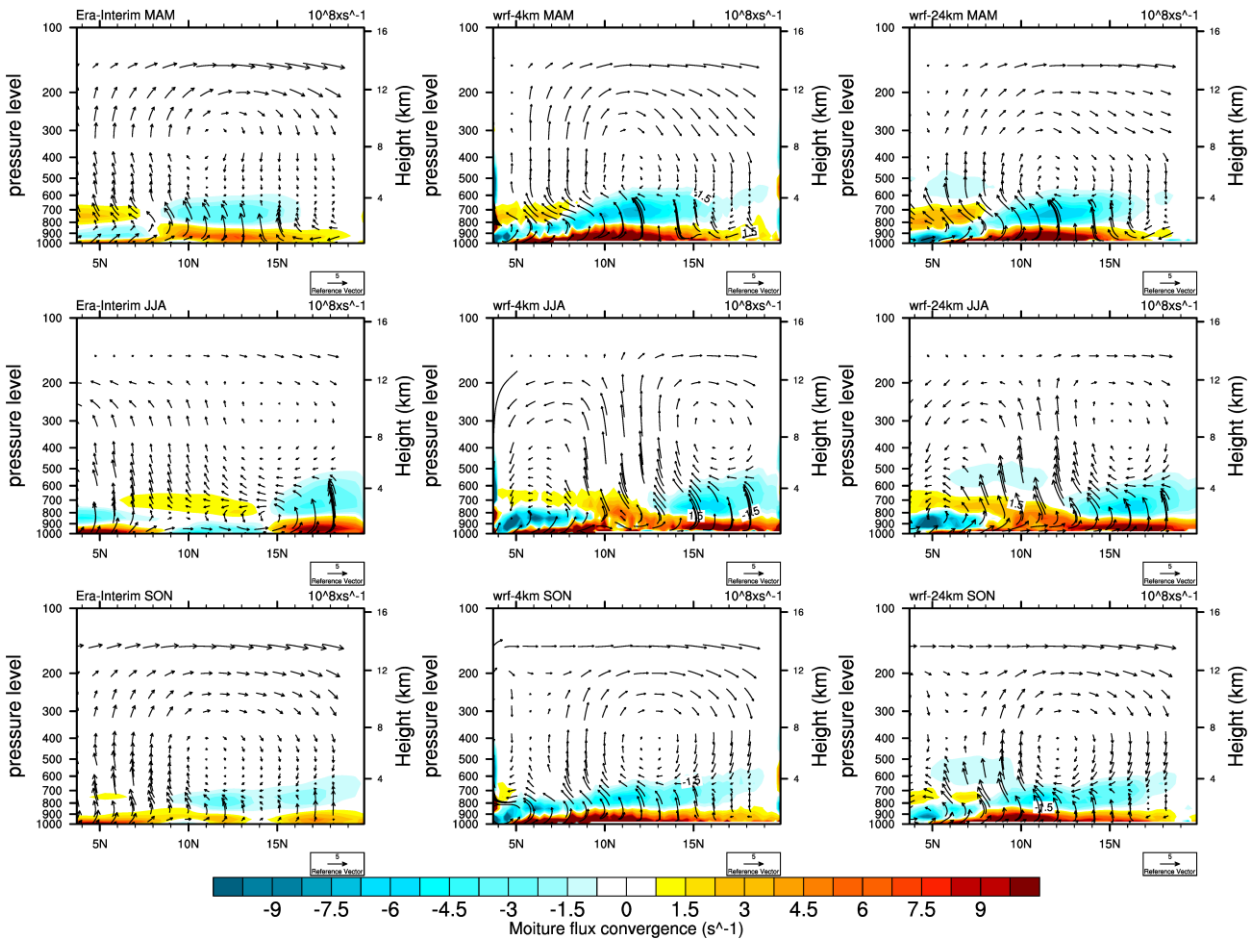


**Fig.7** Seasonal mean of vertical profiles of the moisture flux convergence ( $\times 10^8 s^{-1}$ , in colour) and the meridional (m/s) vertical wind vectors ( $\times 100 Pa \cdot s^{-1}$ ) (v,w). All datasets have been regrided into wrf-24km dataset, averaged for the seasons March-May, June-August and September-November and  $10^{\circ}W$  to  $10^{\circ}E$ . **Column 1** represents ERA-interim; **column 2** and **column 3** represents respectively wrf-4km and wrf-24km.

744

745

746

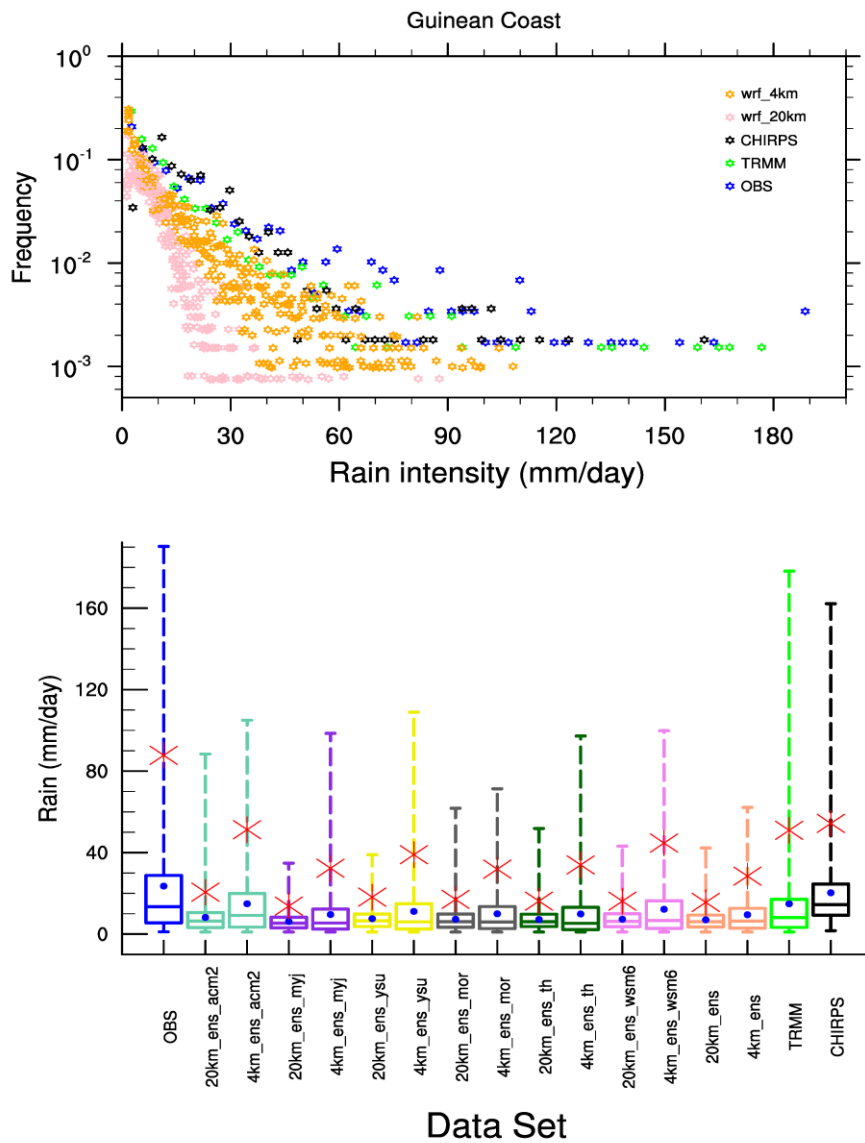


**Fig. 8** Empirical probability distribution functions of daily precipitation (top) daily. Boxplots of the daily precipitation (Bottom) over the Guinean coast (left) and the Sahelian (right) regions. Boxplots of the daily precipitation over the Guinean coast respectively from the ground-based observation, TRMM, ERA-interim and wrf-24km, wrf-4km from each ensemble group members of the different configurations. The boxes indicate respectively from the bottom to the top the first, second and third interquartile ranges and the whiskers stretch to minimum and maximum values of each data set. Blue dots and the red stars represent respectively the mean value and the 95 percentiles of the precipitation for each data set.

747

748

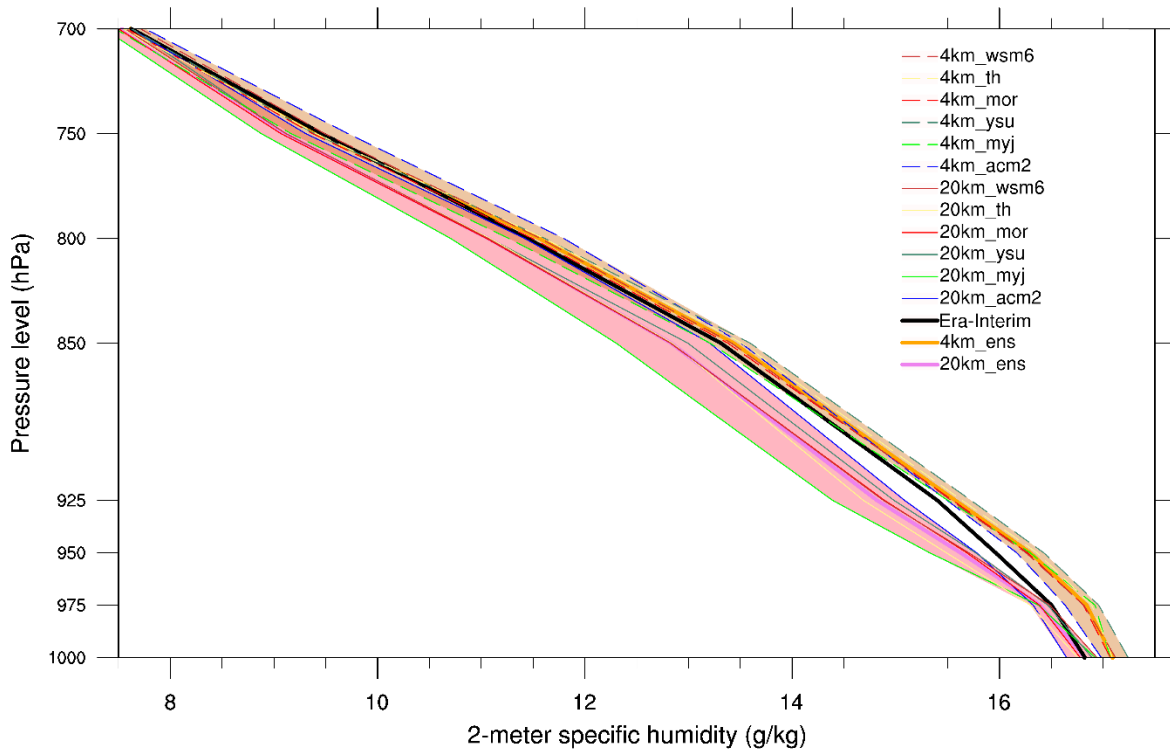


**Fig. 9** Vertical profiles of specific humidity from wrf-20km and 4km sub-ensembles group members and Era-interim data set. All the values are averaged from 10W to 5E. **The pink and orange coloured areas mark the range of value respectively with wrf-24km and wrf4km.**

749

750

751

752

753

754

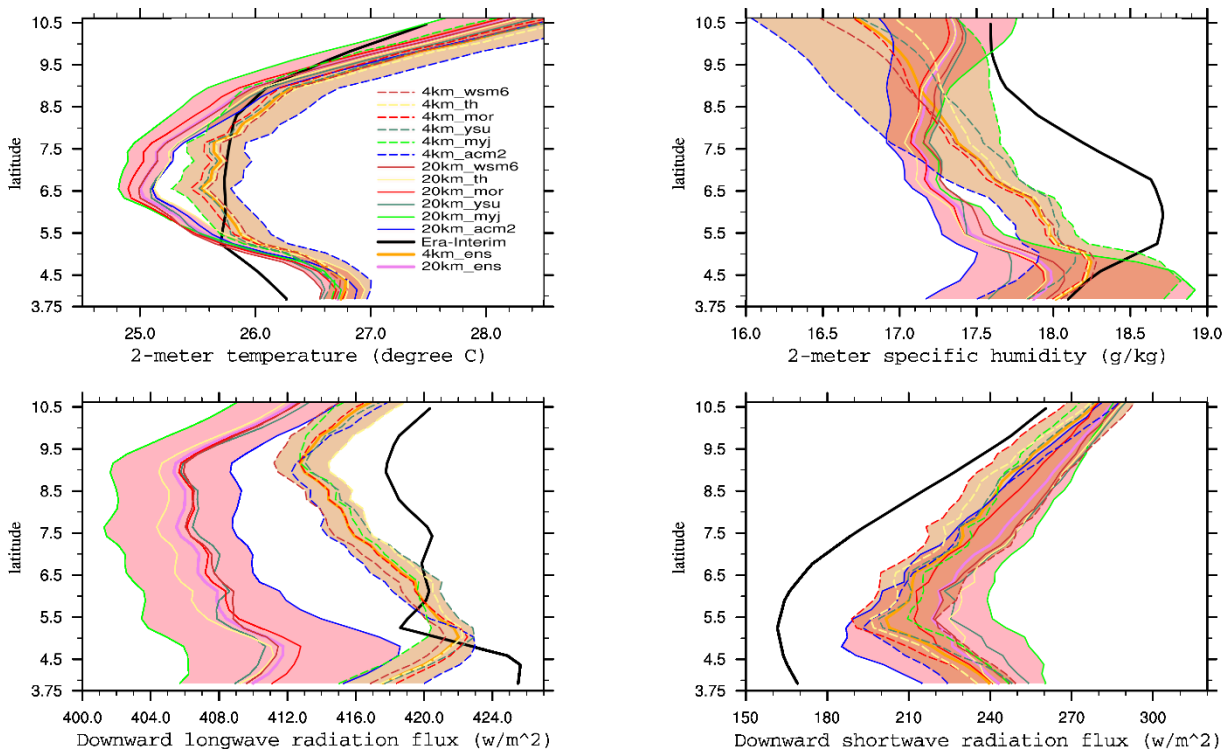


**Fig. 10** Meridional evolution of 2-meter temperature, specific humidity, downward shortwave and longwave radiation fluxes from wrf-20km and 4km ensemble group members and from Era-interim data set. All the values are averaged from 10W to 5 E. The pink and orange coloured areas mark the range of value respectively with wrf-24km and wrf4km.

755

756

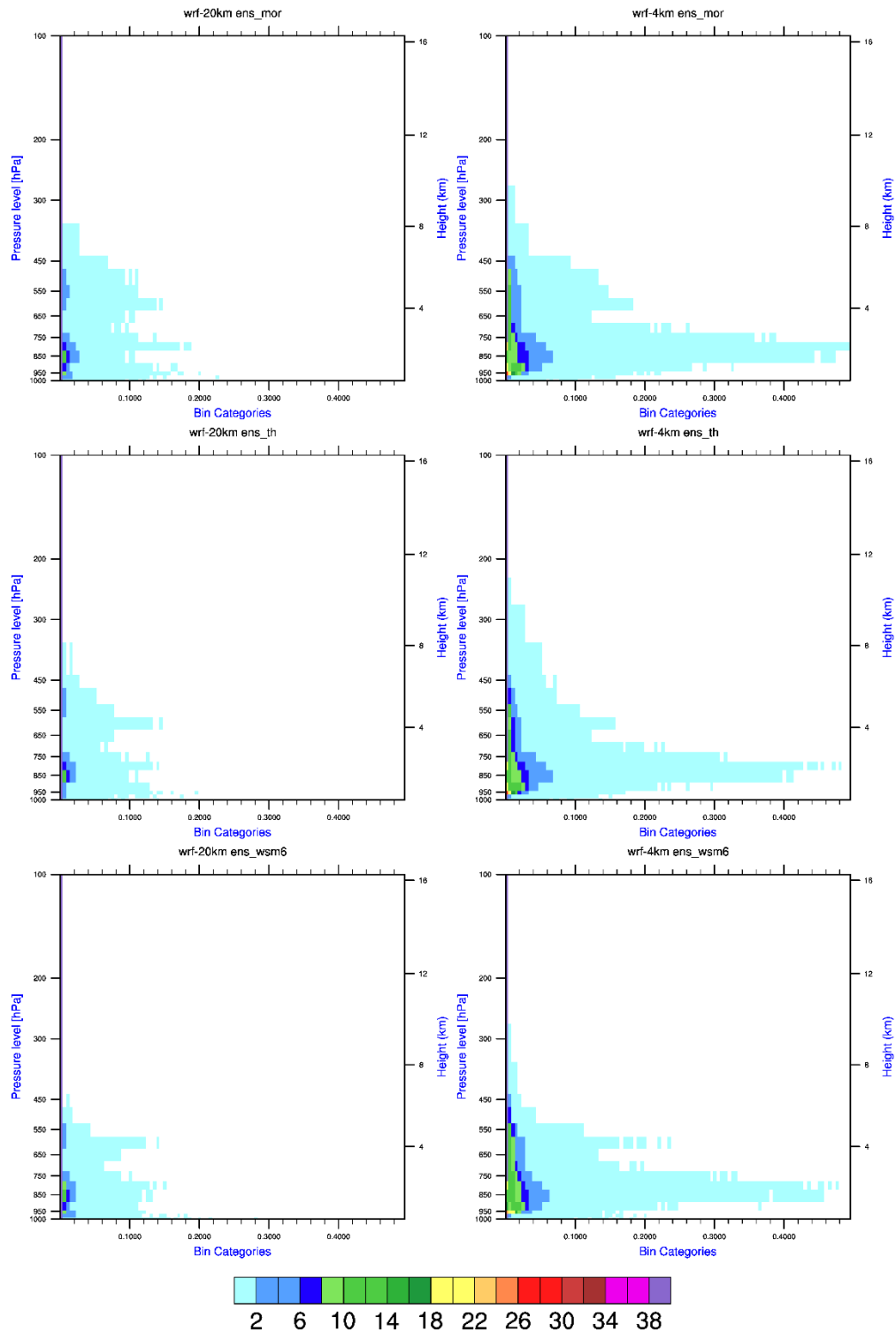


**Fig. 11** Liquid Water Content from wrf-20km and 4km ensemble group members and from Era-interim data set. All the values are averaged from 10W to 5 E.

757  
758

759  
760  
761  
762

## References

- 763 Abiodun BJ, Pal JS, Afiesimama EA, et al (2008) Simulation of West African monsoon using RegCM3  
764 Part II: impacts of deforestation and desertification. *Theor Appl Climatol* 93:245–261
- 765 Adedoyin JA (1989) Global-scale sea-surface temperature anomalies and rainfall characteristics in  
766 northern Nigeria. *Int J Climatol* 9:133–144
- 767 Alapaty K, Herwehe JA, Otte TL, et al (2012) Introducing subgrid-scale cloud feedbacks to radiation for  
768 regional meteorological and climate modeling: CONVECTION AND RADIATION  
769 INTERACTIONS. *Geophys Res Lett* 39:n/a-n/a. doi: 10.1029/2012GL054031
- 770 Ali A, Amani A, Diedhiou A, Lebel T (2005) Rainfall estimation in the Sahel. Part II: Evaluation of rain  
771 gauge networks in the CILSS countries and objective intercomparison of rainfall products. *J Appl*  
772 *Meteorol* 44:1707–1722
- 773 Ban N, Schmidli J, Schär C (2014) Evaluation of the convection-resolving regional climate modeling  
774 approach in decade-long simulations. *J Geophys Res Atmospheres* 119:7889–7907
- 775 Birch CE, Parker DJ, Marsham JH, et al (2014) A seamless assessment of the role of convection in the  
776 water cycle of the West African Monsoon. *J Geophys Res Atmospheres* 119:2890–2912
- 777 Brooks N (2004) Drought in the African Sahel: long term perspectives and future prospects. Tyndall Cent  
778 Clim Change Res Norwich Work Pap 61:31
- 779 Chang C-P (2011) *The Global Monsoon System: Research and Forecast*. World Scientific
- 780 Chen C-T, Knutson T (2008) On the verification and comparison of extreme rainfall indices from climate  
781 models. *J Clim* 21:1605–1621
- 782 Chen F, Dudhia J (2001) Coupling an advanced land surface-hydrology model with the Penn State-NCAR  
783 MM5 modeling system. Part I: Model implementation and sensitivity. *Mon Weather Rev*  
784 129:569–585
- 785 Coëtlogon G de, Janicot S, Lazar A (2010a) Intraseasonal variability of the ocean—atmosphere coupling  
786 in the Gulf of Guinea during boreal spring and summer. *Q J R Meteorol Soc* 136:426–441
- 787 Coëtlogon G de, Janicot S, Lazar A (2010b) Intraseasonal variability of the ocean—atmosphere coupling  
788 in the Gulf of Guinea during boreal spring and summer. *Q J R Meteorol Soc* 136:426–441
- 789 Cook KH (1999) Generation of the African Easterly Jet and Its Role in Determining West African  
790 Precipitation. *J Clim* 12:1165–1184. doi: 10.1175/1520-  
791 0442(1999)012<1165:GOTAEJ>2.0.CO;2
- 792 Dee DP, Uppala SM, Simmons AJ, et al (2011) The ERA-Interim reanalysis: configuration and  
793 performance of the data assimilation system. *Q J R Meteorol Soc* 137:553–597. doi:  
794 10.1002/qj.828

- 795 Di Giuseppe F, Molteni F, Dutra E (2013) Real-time correction of ERA-Interim monthly rainfall.  
796 *Geophys Res Lett* 40:3750–3755
- 797 Di Luca A, de Elía R, Laprise R (2012) Potential for added value in precipitation simulated by high-  
798 resolution nested regional climate models and observations. *Clim Dyn* 38:1229–1247
- 799 Di Luca A, de Elía R, Laprise R (2013) Potential for small scale added value of RCM’s downscaled  
800 climate change signal. *Clim Dyn* 40:601–618. doi: 10.1007/s00382-012-1415-z
- 801 Dirmeyer PA, Cash BA, Kinter III JL, et al (2012) Simulating the diurnal cycle of rainfall in global  
802 climate models: Resolution versus parameterization. *Clim Dyn* 39:399–418
- 803 Doi T, Vecchi GA, Rosati AJ, Delworth TL (2012) Biases in the Atlantic ITCZ in seasonal–interannual  
804 variations for a coarse-and a high-resolution coupled climate model. *J Clim* 25:5494–5511
- 805 Dosio A, Panitz H-J, Schubert-Frisius M, Lüthi D (2014) Dynamical downscaling of CMIP5 global  
806 circulation models over CORDEX-Africa with COSMO-CLM: evaluation over the present  
807 climate and analysis of the added value. *Clim Dyn* 44:2637–2661. doi: 10.1007/s00382-014-  
808 2262-x
- 809 Druyan LM, Feng J, Cook KH, et al (2010) The WAMME regional model intercomparison study. *Clim*  
810 *Dyn* 35:175–192. doi: 10.1007/s00382-009-0676-7
- 811 Dudhia J (1989) Numerical study of convection observed during the winter monsoon experiment using a  
812 mesoscale two-dimensional model. *J Atmospheric Sci* 46:3077–3107
- 813 Emori S, Hasegawa A, Suzuki T, Dairaku K (2005) Validation, parameterization dependence, and future  
814 projection of daily precipitation simulated with a high-resolution atmospheric GCM. *Geophys*  
815 *Res Lett* 32:
- 816 Evan AT, Flamant C, Lavaysse C, et al (2015) Water vapor–forced greenhouse warming over the Sahara  
817 Desert and the recent recovery from the Sahelian drought. *J Clim* 28:108–123
- 818 Fink AH, Schrage JM, Kotthaus S (2010) On the potential causes of the nonstationary correlations  
819 between West African precipitation and Atlantic hurricane activity. *J Clim* 23:5437–5456
- 820 Flaounas E, Bastin S, Janicot S (2011) Regional climate modelling of the 2006 West African monsoon:  
821 sensitivity to convection and planetary boundary layer parameterisation using WRF. *Clim Dyn*  
822 36:1083–1105
- 823 Flaounas E, Janicot S, Bastin S, Roca R (2012) The West African monsoon onset in 2006: sensitivity to  
824 surface albedo, orography, SST and synoptic scale dry-air intrusions using WRF. *Clim Dyn*  
825 38:685–708
- 826 Fontaine B, Louvet S, Roucou P (2008) Definition and predictability of an OLR based West African  
827 monsoon onset. *Int J Climatol* 28:1097–1798
- 828 Fontaine B, Philippon N (2000) Seasonal evolution of boundary layer heat content in the West African  
829 monsoon from the NCEP/NCAR reanalysis (1968–1998). *Int J Climatol* 20:1777–1790

- 830 Funk C, Peterson P, Landsfeld M, et al (2015) The climate hazards infrared precipitation with stations—a  
831 new environmental record for monitoring extremes. *Sci Data* 2:150066
- 832 Gaetani M, Flamant C, Bastin S, et al (2017) West African monsoon dynamics and precipitation: the  
833 competition between global SST warming and CO2 increase in CMIP5 idealized simulations.  
834 *Clim Dyn* 48:1353–1373
- 835 Gallée H, Moufouma-Okia W, Bechtold P, et al (2004) A high-resolution simulation of a West African  
836 rainy season using a regional climate model. *J Geophys Res Atmospheres* 109:D05108. doi:  
837 10.1029/2003JD004020
- 838 Gbobaniyi E, Sarr A, Sylla MB, et al (2014) Climatology, annual cycle and interannual variability of  
839 precipitation and temperature in CORDEX simulations over West Africa. *Int J Climatol* 34:2241–  
840 2257
- 841 Griggs DJ, Noguer M (2002) Climate change 2001: the scientific basis. Contribution of working group I  
842 to the third assessment report of the intergovernmental panel on climate change. *Weather* 57:267–  
843 269
- 844 Grist JP, Nicholson SE (2001) A study of the dynamic factors influencing the rainfall variability in the  
845 West African Sahel. *J Clim* 14:1337–1359
- 846 Hagos SM, Cook KH (2007) Dynamics of the West African Monsoon Jump. *J Clim* 20:5264–5284. doi:  
847 10.1175/2007JCLI1533.1
- 848 Harlaß J, Latif M, Park W (2017) Alleviating tropical Atlantic sector biases in the Kiel climate model by  
849 enhancing horizontal and vertical atmosphere model resolution: climatology and interannual  
850 variability. *Clim Dyn* 1–31
- 851 Herwehe JA, Alapaty K, Spero TL, Nolte CG (2014) Increasing the credibility of regional climate  
852 simulations by introducing subgrid-scale cloud-radiation interactions: RCM sims with Cu-  
853 radiation interactions. *J Geophys Res Atmospheres* 119:5317–5330. doi: 10.1002/2014JD021504
- 854 Holloway CE, Neelin JD (2009) Moisture vertical structure, column water vapor, and tropical deep  
855 convection. *J Atmospheric Sci* 66:1665–1683
- 856 Holloway CE, Woolnough SJ, Lister GMS (2012) Precipitation distributions for explicit versus  
857 parametrized convection in a large-domain high-resolution tropical case study. *Q J R Meteorol*  
858 *Soc* 138:1692–1708
- 859 Holtslag AAM, Boville BA (1993) Local versus nonlocal boundary-layer diffusion in a global climate  
860 model. *J Clim* 6:1825–1842
- 861 Hong S-Y, Lim J-OJ (2006) The WRF single-moment 6-class microphysics scheme (WSM6). *J Korean*  
862 *Meteor Soc* 42:129–151
- 863 Hong S-Y, Noh Y, Dudhia J (2006) A new vertical diffusion package with an explicit treatment of  
864 entrainment processes. *Mon Weather Rev* 134:2318–2341

- 865 Huffman GJ, Bolvin DT, Nelkin EJ, et al (2007) The TRMM Multisatellite Precipitation Analysis  
866 (TMPA): Quasi-Global, Multiyear, Combined-Sensor Precipitation Estimates at Fine Scales. *J*  
867 *Hydrometeorol* 8:38–55. doi: 10.1175/JHM560.1
- 868 Iorio JP, Duffy PB, Govindasamy B, et al (2004) Effects of model resolution and subgrid-scale physics on  
869 the simulation of precipitation in the continental United States. *Clim Dyn* 23:243–258
- 870 Janicot S, Mounier F, Gervois S, et al (2010) The dynamics of the West African monsoon. Part V: The  
871 detection and role of the dominant modes of convectively coupled equatorial Rossby waves. *J*  
872 *Clim* 23:4005–4024
- 873 Janjic ZI (1994) The step-mountain eta coordinate model: Further developments of the convection,  
874 viscous sublayer, and turbulence closure schemes. *Mon Weather Rev* 122:927–945
- 875 Janjić ZI (2002) Nonsingular implementation of the Mellor–Yamada level 2.5 scheme in the NCEP Meso  
876 model. *NCEP Off Note* 437:61
- 877 Kharin VV, Zwiers FW, Zhang X (2005) Intercomparison of near-surface temperature and precipitation  
878 extremes in AMIP-2 simulations, reanalyses, and observations. *J Clim* 18:5201–5223
- 879 Klein C, Heinzeller D, Bliefernicht J, Kunstmann H (2015) Variability of West African monsoon patterns  
880 generated by a WRF multi-physics ensemble. *Clim Dyn* 1–23
- 881 Konare A, Zakey AS, Solmon F, et al (2008) A regional climate modeling study of the effect of desert  
882 dust on the West African monsoon. *J Geophys Res* 113:. doi: 10.1029/2007JD009322
- 883 Laprise R, De Elia R, Caya D, et al (2008) Challenging some tenets of regional climate modelling.  
884 *Meteorol Atmospheric Phys* 100:3–22
- 885 Lavaysse C, Diedhiou A, Laurent H, Lebel T (2006) African Easterly Waves and convective activity in  
886 wet and dry sequences of the West African Monsoon. *Clim Dyn* 27:319–332
- 887 Lavaysse C, Flamant C, Janicot S, et al (2009) Seasonal evolution of the West African heat low: a  
888 climatological perspective. *Clim Dyn* 33:313–330. doi: 10.1007/s00382-009-0553-4
- 889 Lavaysse C, Flamant C, Janicot S (2010a) Regional-scale convection patterns during strong and weak  
890 phases of the Saharan heat low. *Atmospheric Sci Lett* 11:255–264
- 891 Lavaysse C, Flamant C, Janicot S, Knippertz P (2010b) Links between African easterly waves,  
892 midlatitude circulation and intraseasonal pulsations of the West African heat low. *Q J R Meteorol*  
893 *Soc* 136:141–158
- 894 Lebel T, Diedhiou A, Laurent H (2003) Seasonal cycle and interannual variability of the Sahelian rainfall  
895 at hydrological scales. *J Geophys Res Atmospheres* 1984–2012 108:
- 896 Leduc-Leballeur M, De Coëtlogon G, Eymard L (2013) Air–sea interaction in the Gulf of Guinea at  
897 intraseasonal time-scales: wind bursts and coastal precipitation in boreal spring. *Q J R Meteorol*  
898 *Soc* 139:387–400
- 899 Leduc-Leballeur M, Eymard L, De Coëtlogon G (2011) Observation of the marine atmospheric boundary  
900 layer in the Gulf of Guinea during the 2006 boreal spring. *Q J R Meteorol Soc* 137:992–1003

- 901 Lind P, Lindstedt D, Kjellström E, Jones C (2016) Spatial and Temporal Characteristics of Summer  
 902 Precipitation over Central Europe in a Suite of High-Resolution Climate Models. *J Clim*  
 903 29:3501–3518. doi: 10.1175/JCLI-D-15-0463.1
- 904 Marsham JH, Dixon NS, Garcia-Carreras L, et al (2013) The role of moist convection in the West African  
 905 monsoon system: Insights from continental-scale convection-permitting simulations. *Geophys*  
 906 *Res Lett* 40:1843–1849
- 907 Meynadier R, Bock O, Gervois S, et al (2010) West African Monsoon water cycle: 2. Assessment of  
 908 numerical weather prediction water budgets. *J Geophys Res Atmospheres* 115:1984–2012
- 909 Meynadier R, De Coëtlogon G, Bastin S, et al (2014) Sensitivity testing of WRF parameterizations on  
 910 air–sea interaction and its impact on water cycle in the Gulf of Guinea. *Q J R Meteorol Soc*
- 911 Mlawer EJ, Taubman SJ, Brown PD, et al (1997) Radiative transfer for inhomogeneous atmospheres:  
 912 RRTM, a validated correlated-k model for the longwave. *J Geophys Res Atmospheres* 102:16663–16682
- 914 Mohino E, Rodríguez-Fonseca B, Mechoso CR, et al (2011) Impacts of the tropical Pacific/Indian Oceans  
 915 on the seasonal cycle of the West African monsoon. *J Clim* 24:3878–3891
- 916 Morrison H, Thompson G, Tatarskii V (2009) Impact of cloud microphysics on the development of  
 917 trailing stratiform precipitation in a simulated squall line: Comparison of one-and two-moment  
 918 schemes. *Mon Weather Rev* 137:991–1007
- 919 Moufouma-Okia W, Jones R (2014) Resolution dependence in simulating the African hydroclimate with  
 920 the HadGEM3-RA regional climate model. *Clim Dyn* 1–24
- 921 Moufouma-Okia W, Rowell DP (2010) Impact of soil moisture initialisation and lateral boundary  
 922 conditions on regional climate model simulations of the West African Monsoon. *Clim Dyn*  
 923 35:213–229
- 924 Neelin JD, Peters O, Hales K (2009) The Transition to Strong Convection. *J Atmospheric Sci* 66:2367–  
 925 2384. doi: 10.1175/2009JAS2962.1
- 926 Nicholson SE (2001) Climatic and environmental change in Africa during the last two centuries. *Clim*  
 927 *Res* 17:123–144
- 928 Nicholson SE (2013a) The West African Sahel: A review of recent studies on the rainfall regime and its  
 929 interannual variability. *ISRN Meteorol* 2013:
- 930 Nicholson SE (2013b) The West African Sahel: A review of recent studies on the rainfall regime and its  
 931 interannual variability. *ISRN Meteorol* 2013:
- 932 Nicholson SE (2008) The intensity, location and structure of the tropical rainbelt over west Africa as  
 933 factors in interannual variability. *Int J Climatol* 28:1775–1785. doi: 10.1002/joc.1507
- 934 Nicholson SE (2009) A revised picture of the structure of the “monsoon” and land ITCZ over West  
 935 Africa. *Clim Dyn* 32:1155–1171

- 936 Nicholson SE (2013c) The West African Sahel: A review of recent studies on the rainfall regime and its  
937 interannual variability. ISRN Meteorol 2013:
- 938 Nicholson SE, Dezfuli AK, Klotter D (2012) A two-century precipitation dataset for the continent of  
939 Africa. Bull Am Meteorol Soc 93:1219–1231
- 940 Nicholson SE, Grist JP (2003) The seasonal evolution of the atmospheric circulation over West Africa  
941 and equatorial Africa. J Clim 16:1013–1030
- 942 Oettli P, Sultan B, Baron C, Vrac M (2011) Are regional climate models relevant for crop yield prediction  
943 in West Africa? Environ Res Lett 6:14008
- 944 Okumura Y, Xie S-P (2004) Interaction of the Atlantic Equatorial Cold Tongue and the African  
945 Monsoon\*. J Clim 17:3589–3602
- 946 Omotosho JB (2008) Pre-rainy season moisture build-up and storm precipitation delivery in the West  
947 African Sahel. Int J Climatol 28:937–946. doi: 10.1002/joc.1548
- 948 Omotosho JB, Balogun AA, Ogunjobi K, others (2000) Predicting monthly and seasonal rainfall, onset  
949 and cessation of the rainy season in West Africa using only surface data. Int J Climatol 20:865–  
950 880
- 951 Omrani H, Drobinski P, Dubos T (2012) Spectral nudging in regional climate modelling: how strongly  
952 should we nudge? Q J R Meteorol Soc 138:1808–1813
- 953 Panitz H-J, Dosio A, Büchner M, et al (2014) COSMO-CLM (CCLM) climate simulations over  
954 CORDEX-Africa domain: analysis of the ERA-Interim driven simulations at 0.44 and 0.22  
955 resolution. Clim Dyn 42:3015–3038
- 956 Patricola CM, Li M, Xu Z, et al (2012) An investigation of tropical Atlantic bias in a high-resolution  
957 coupled regional climate model. Clim Dyn 39:2443–2463
- 958 Pleim JE (2007) A combined local and nonlocal closure model for the atmospheric boundary layer. Part  
959 II: Application and evaluation in a mesoscale meteorological model. J Appl Meteorol Climatol  
960 46:1396–1409
- 961 Pm. Ruti AD (2009) How do the large-scale models represent the West African intra-seasonal variability  
962 and its relationship with remote or local forcing
- 963 Pohl B, Crétat J, Camberlin P (2011) Testing WRF capability in simulating the atmospheric water cycle  
964 over Equatorial East Africa. Clim Dyn 37:1357–1379
- 965 Prein AF, Langhans W, Fosser G, et al (2015) A review on regional convection-permitting climate  
966 modeling: Demonstrations, prospects, and challenges. Rev Geophys 53:323–361
- 967 Salameh T, Drobinski P, Dubos T (2010) The effect of indiscriminate nudging time on large and small  
968 scales in regional climate modelling: application to the Mediterranean basin. Q J R Meteorol Soc  
969 136:170–182
- 970 Small RJ, Bacmeister J, Bailey D, et al (2014) A new synoptic scale resolving global climate simulation  
971 using the Community Earth System Model. J Adv Model Earth Syst 6:1065–1094

972 Stauffer DR, Seaman NL (1990) Use of four-dimensional data assimilation in a limited-area mesoscale  
973 model. Part I: Experiments with synoptic-scale data. *Mon Weather Rev* 118:1250–1277

974 Steiner AL, Pal JS, Rauscher SA, et al (2009) Land surface coupling in regional climate simulations of  
975 the West African monsoon. *Clim Dyn* 33:869–892

976 Stephens GL, L’Ecuyer T, Forbes R, et al (2010) Dreary state of precipitation in global models. *J*  
977 *Geophys Res Atmospheres* 115:

978 Sultan B, Janicot S (2000) Abrupt shift of the ITCZ over West Africa and intra-seasonal variability.  
979 *Geophys Res Lett* 27:3353–3356

980 Sultan B, Janicot S (2003) The West African monsoon dynamics. Part II: The “preonset” and “onset” of  
981 the summer monsoon. *J Clim* 16:3407–3427

982 Sultan B, Janicot S, Diedhiou A (2003) The West African monsoon dynamics. Part I: Documentation of  
983 intraseasonal variability. *J Clim* 16:3389–3406

984 Sylla MB, Coppola E, Mariotti L, et al (2010a) Multiyear simulation of the African climate using a  
985 regional climate model (RegCM3) with the high resolution ERA-interim reanalysis. *Clim Dyn*  
986 35:231–247

987 Sylla MB, Dell’Aquila A, Ruti PM, Giorgi F (2010b) Simulation of the intraseasonal and the interannual  
988 variability of rainfall over West Africa with RegCM3 during the monsoon period. *Int J Climatol*  
989 30:1865–1883

990 Tao W-K, Moncrieff MW (2009) Multiscale cloud system modeling. *Rev Geophys* 47:

991 Thompson G, Field PR, Rasmussen RM, Hall WD (2008) Explicit forecasts of winter precipitation using  
992 an improved bulk microphysics scheme. Part II: Implementation of a new snow parameterization.  
993 *Mon Weather Rev* 136:5095–5115

994 Trenberth KE, Stepaniak DP, Caron JM (2000) The global monsoon as seen through the divergent  
995 atmospheric circulation. *J Clim* 13:3969–3993

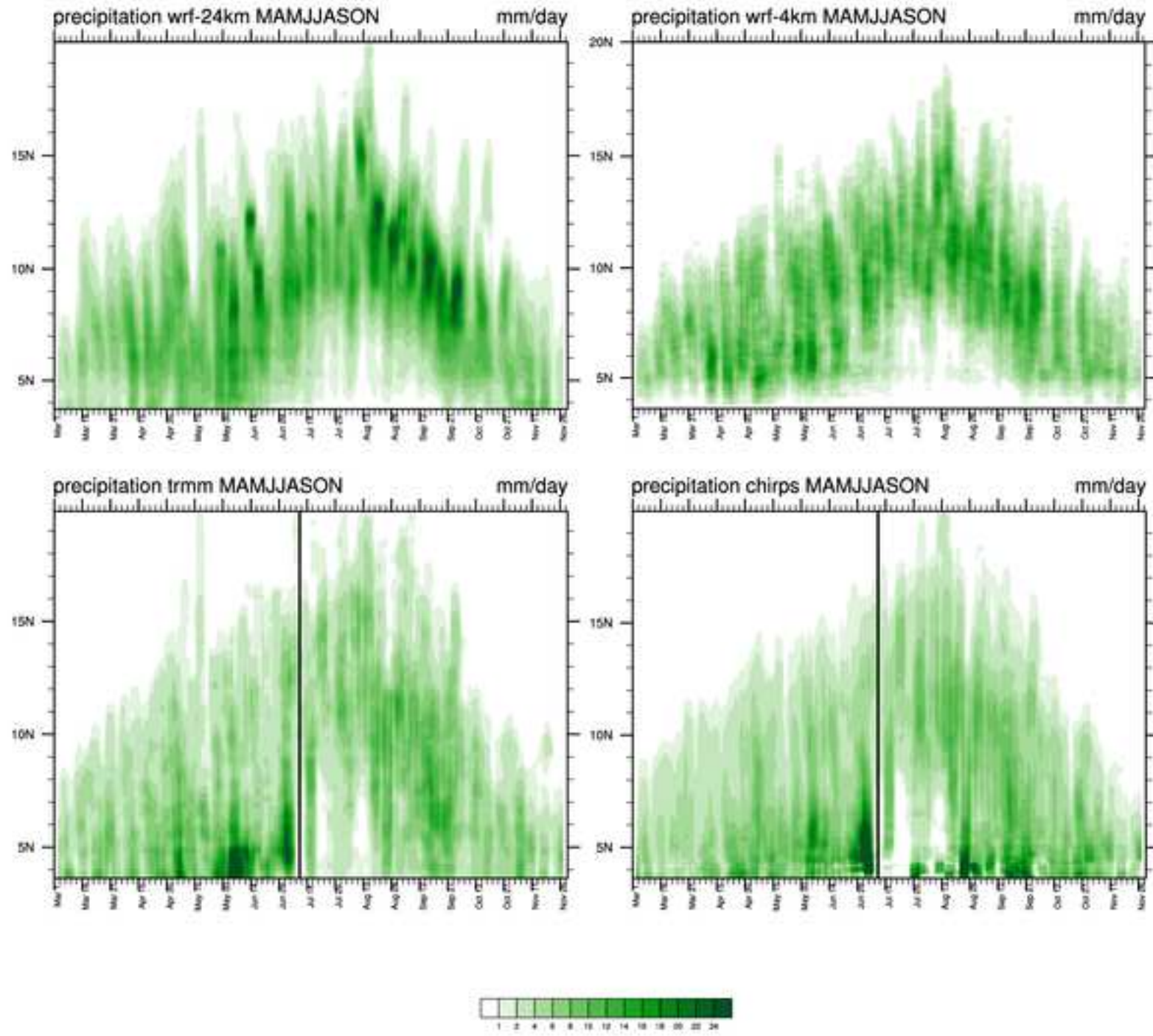
996 Vizio EK (2002) Development and application of a mesoscale climate model for the tropics: Influence of  
997 sea surface temperature anomalies on the West African monsoon. *J Geophys Res* 107:. doi:  
998 10.1029/2001JD000686

999 Xie B, Fung JC, Chan A, Lau A (2012) Evaluation of nonlocal and local planetary boundary layer  
1000 schemes in the WRF model. *J Geophys Res Atmospheres* 117:1984–2012 117:

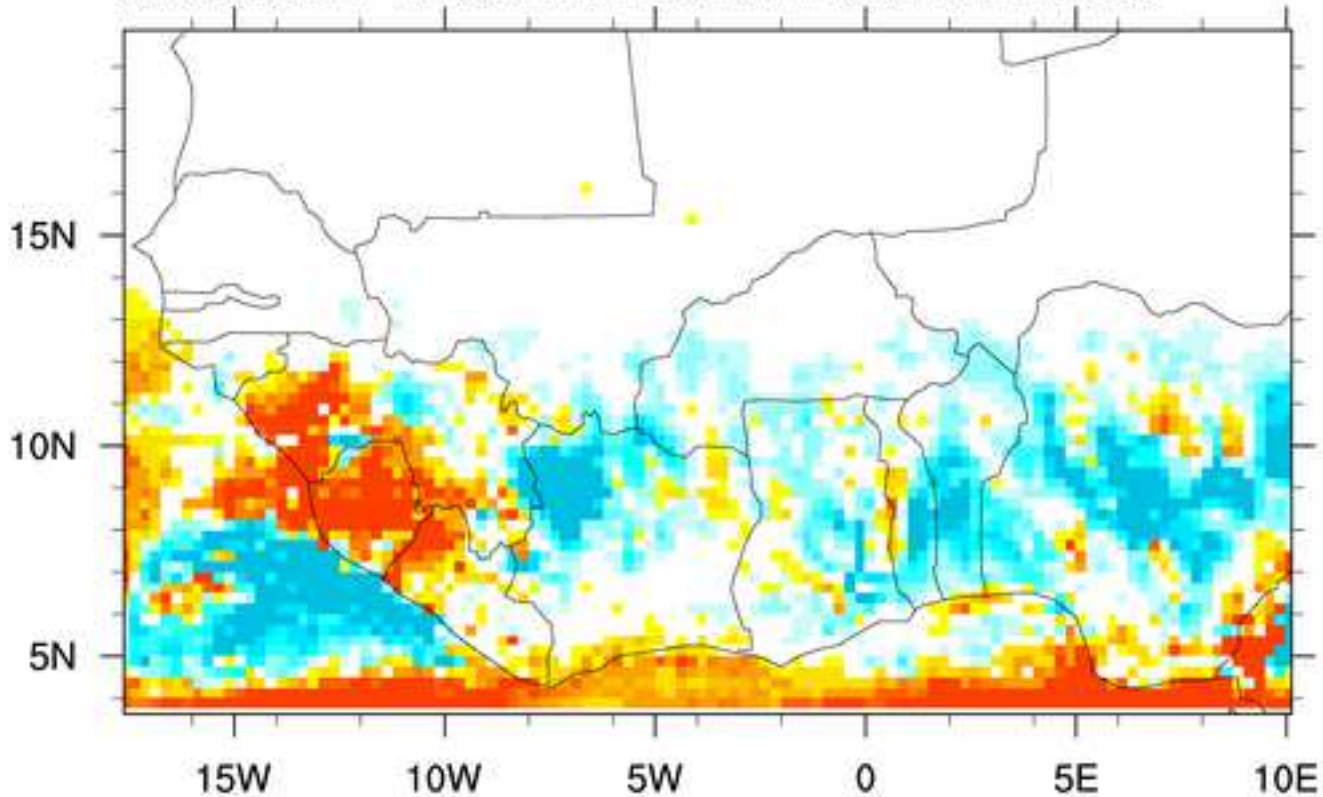
1001 Zhang C, Woodworth P, Gu G (2006) The seasonal cycle in the lower troposphere over West Africa from  
1002 sounding observations. *Q J R Meteorol Soc* 132:2559–2582

1003





added value WRF-4km to wrf-24km mean March-November trmm as ref.



added value WRF-4km to wrf-24km mean March-November chirps as ref.

